Graz University of Technology
Institute of Applied Mechanics

AM:BM

Preprint Series

Preprint No 01/2019

Space-Time discretized Retarded Potential Boundary Integral Operators: Quadrature for Collocation Methods

Dominik Pölz, Martin Schanz
Institute of Applied Mechanics, Graz University of Technology

Submitted to: *SIAM Journal on Scientific Computing*
Latest revision: February 25, 2019

Abstract

We propose a novel discretization method for time domain boundary integral equations of the 3d wave equation. The basic idea of the discussed approach is to treat time as if it were an additional spatial coordinate. This leads to a discretization of the boundary integral operators in 3+1 dimensional space-time by use of basis functions which do not separate space and time variables. These functions are based on tetrahedral meshes of the lateral boundary of the space-time cylinder. An explicit representation of the integral operators of the wave equation, so-called retarded potential integral operators, appropriate for space-time trial functions is discussed. The majority of this work is concerned with the numerical evaluation of these integrals. An accurate and robust Gaussian quadrature scheme is proposed and verified by means of numerical experiments.

1 Introduction

The study of transient wave propagation processes plays a key role in various fields of modern engineering and applied sciences. In particular, the linear wave equation is a viable model for acoustic as well as electromagnetic waves in many situations. An important class of problems related to these types of waves are scattering problems, where the scattered wave field in the unbounded exterior of the scatterer is of interest. For such problems the boundary integral equation method is a promising approach, as it reduces the problem posed on the unbounded exterior to the bounded surface of the scatterer. Due to causality and finite speed of propagation the integral operators associated to the wave equation have a special structure, motivating the prominent term retarded potential boundary integral equations (RPBIE).

The inherent advantages of boundary integral equations in transient scattering problems inspired numerous publications dedicated towards their analysis and their discretization. The mathematical analysis of integral equations of hyperbolic problems was sparked by the seminal publications of Bamberger and Ha-Duong [4, 5]. In their approach, the authors apply the Laplace transform with respect to the time variable to the wave equation and related boundary integral equations. The behaviour of the solution of the transformed equations is estimated with respect to the frequency and the results are transported to time domain by inverse Laplace transform. The review paper of Ha-Duong [33] and the book of Sayas [64] provide particularly elegant overviews of the results obtained by this method. In contrast to this classical approach, Sayas [63, 64] develops a time domain analysis, based on the theory of semigroups of operators, which leads to better estimates. Moreover, Rynne [58] analyses a related problem arising in electrodynamics via a time domain technique based on the theory of hyperbolic equations. This approach yields better estimates than the ones due to Bamberger and Ha-Duong, however, requires smoothness of the boundary. The article of Joly and Rodríguez [35] provides a thorough review and discussion of the existing literature and analyses different bilinear forms of RPBIEs.

1.1 Boundary element methods for RPBIEs

Approximation techniques for RPBIEs can be traced back to Friedman and Shaw [21]. Mansur [46] developed the first boundary element method in the modern sense. The review article of Costabel and Sayas [11] and the preface in [64] present an excellent overview of the available literature. The following paragraphs attempt to provide a non-exhaustive overview of prominent boundary element methods for time domain integral equations.

As already mentioned, the first and perhaps most straightforward class of discretization schemes for RPBIEs has its origins in the work of Mansur [47, 46]. Within these procedures an ansatz for the unknown surface density is constructed as a product of separate ansatz functions in the space and time variable, see e.g. [10]. The RPBIE is collocated, i.e. interpolated, at certain collocation points on the spatial grid and at fixed time steps. Due to inherent stability issues of these schemes [56, 59], several articles have been devoted towards their stabilization [57, 14, 13, 12].

A substantially more intricate approach to solving time domain integral equations is constituted by Galerkin methods based on space-time variational formulations of RPBIEs. The stability of these procedures is due to coercivity properties of certain bilinear forms associated to first kind RPBIEs, first established in [4]. Due to their favourable properties, many articles

were dedicated towards the development of Galerkin methods [29, 1, 60, 8, 68, 27, 28].

While the first two approaches deal with time domain boundary integral equations directly, there exist methods that circumvent the intricate implementation of RPBIEs. A distinguished discretization scheme goes back to Lubich's convolution quadrature method (CQM) [42, 43]. The convolution type time domain integral operators are computed with the CQM and the integral equation is satisfied at equally spaced points in time. This approach is combined with well-established boundary element methods for stationary problems, e.g. collocation or Galerkin methods [44, 7, 6, 3]. Decisive advantages of these approaches are their inherent stability properties and the fact that the fundamental solution of the partial differential operator has to be known in Laplace domain only, cf. [66]. In the recent past this approach has been extended to enable variable time step sizes [39, 40, 41].

Moreover, there are boundary element methods for the wave equation that entirely avoid the use of retarded potentials. In a variant of Rothe's method [55] the initial-boundary value problem is discretized in time with a suitable implicit time-stepping scheme. The resulting stationary problem at each time step is solved by well-established boundary element methods for elliptic problems, see [11].

A common feature of virtually any yet implemented boundary element method for the wave equation is that they discretize space and time separately. In contrast, we seek to take a first step towards the development of a genuine space-time discretization method in this paper. The following paragraphs exhibit basic concepts and existing literature on the space-time methodology.

1.2 Space-time methodology

The basic idea of space-time methods is to treat the time variable as if it were an additional spatial coordinate. This thinking suggests to treat the transient problem as a single operator equation in space-time even within the discretization. Consequently, one is confronted with a $d+1$ dimensional computational domain, where $d \in \mathbb{N}$ is the number of spatial dimensions. This domain can be decomposed into finite elements in an unstructured fashion, i.e. without distinguishing between space and time dimensions. Such an *unstructured* discretization of the space-time domain is, at least from our point of view, the distinguishing feature of space-time discretization methods. In [34], an elegant illustration of this methodology in $1+1$ dimensions is presented. The development of space-time finite element methods has already reached a certain degree of maturity, see e.g. [49, 67, 24, 50, 15, 69] and [18, 31, 32] for recent advances. The major drawback of space-time methods is their increased demand in terms of computational resources compared to classical approaches based on semi-discretization. Since the problem is discretized in $d+1$ dimensions, generally larger systems have to be stored as well as solved. Nevertheless, space-time methods possess several crucial advantages:

- Flexible space-time meshes can adapt locally to special features of the solution, such as wave fronts. Adaptivity within space-time boundary element methods for the 1d wave equation is explored in [71, 53]. In fact, the results exhibited in these publications serve as prime impetus for this work on the 3d wave equation.

- Problems posed on instationary domains are treated naturally since the deformed configuration of the domain at any point in time is captured by the space-time mesh itself

[49, 70].

- Considering the discretized transient problem as one operator equation in space-time enables the application of parallel solution strategies in both space and time, cf. [49, 24].

On the other hand, there has been hardly any development of space-time discretization schemes for time domain integral equations. The integral representations of these operators are quite involved, especially in the case of hyperbolic problems. However, there exist techniques for computing these integrals if space and time are treated separately, see e.g. [2, 26]. The intricacy of computing integral operators for unstructured space-time decompositions is why, to the best of our knowledge, any yet implemented discretization scheme for RPBIEs features a product structure in space and time. We emphasize that unstructured space-time meshes as well as instationary boundaries in the context of integral equations of parabolic problems are examined in recent publications [17, 45].

The novelty of this paper lies in the utilization of space-time trial functions that are *not* products of functions in space and functions in time for RPBIEs. The employed trial functions stem from standard finite element spaces defined on tetrahedral meshes of the lateral boundary of the space-time cylinder. This approach inherits the advantages of the space-time methodology, however, the integrals of the retarded layer potentials are quite complicated within this approach. That is why we restrict our considerations in this paper to collocation approaches, which we label space-time collocation schemes. The major part of this contribution is dedicated towards a numerical integration technique for the computation of the arising integrals. We provide an accurate quadrature technique for the evaluation of retarded layer integral operators that relies on an explicit parametrization of the integration surface in reference coordinates. The employed parametrization, however, is only available for flat space-time boundary elements. To the best of our knowledge, this paper provides the first implementation and numerical computations of a method for RPBIEs in $3+1$ dimensions using unstructured space-time meshes.

The paper is organized as follows. In Section 2 the considered model initial-boundary value problem is discussed. Furthermore, the related time domain boundary integral equations are provided. Section 3 exposes the proposed space-time collocation method for the RPBIEs of the preceding section. The standard integral representations of retarded layer integral operators are recast to a form appropriate for the chosen space-time trial functions. A numerical integration scheme for the occurring, quite intricate, integrals is proposed. In Section 4 the integration technique and the overall collocation method are verified by means of numerical examples. Section 5 concludes this paper by summarizing the findings and addressing critical issues of the proposed approach.

2 Integral form of the wave equation

Let $\Omega^- \subset \mathbb{R}^3$ be a bounded open domain with Lipschitz boundary $\Gamma := \partial\Omega^-$ and exterior $\Omega^+ := \mathbb{R}^3 \setminus \overline{\Omega^-}$. The vector field $n : \Gamma \to \mathbb{R}^3$ represents the unit outward normal vector of Γ, which points towards Ω^+. Moreover, let $c > 0$ be the wave velocity, e.g. the speed of sound for acoustic waves. In this work we employ the scaled time coordinate $t = ct^*$, where t^* is the physical time. For a fixed physical simulation end time $T^* > 0$ we define $T = cT^*$ and the space-time cylinder

$Q^+ := (0,T) \times \Omega^+$ with lateral boundary $\Sigma := (0,T) \times \Gamma$. We are concerned with solutions of the homogeneous wave equation

$$\partial_t^2 u - \Delta_x u = 0 \quad \text{in } Q^+ \tag{1}$$

where Δ_x denotes the the Laplacian with respect to the spatial coordinates. The solution is subject to homogeneous initial conditions

$$u = 0 \ \wedge \ \partial_t u = 0 \quad \text{on } \{0\} \times \Omega^+. \tag{2}$$

To impose boundary conditions we make use of the trace operator, which is for a sufficiently smooth function $f : Q^+ \to \mathbb{R}$ defined by

$$\gamma_0^+ f(t,x) = \lim_{\Omega^+ \ni y \to x \in \Gamma} f(t,y), \quad (t,x) \in \Sigma.$$

Moreover, the normal derivative is denoted by

$$\gamma_1^+ f = \langle n, \gamma_0^+ \nabla_x f \rangle$$

where ∇_x is the gradient with respect to the spatial coordinates and $\langle \cdot, \cdot \rangle$ is the Euclidean scalar product with induced norm $\langle \cdot, \cdot \rangle = \| \cdot \|^2$. We consider boundary conditions of Dirichlet type: For given Dirichlet datum g the solution u has to satisfy

$$\gamma_0^+ u = g \quad \text{on } \Sigma. \tag{3}$$

The solution of the initial-boundary value problem Eqs. (1) to (3) can be represented by boundary integrals in an elegant fashion, since they reduce the problem posed on the unbounded domain Q^+ to the bounded lateral boundary Σ. For sufficiently smooth surface densities $w, v : \Sigma \to \mathbb{R}$ and $(t,x) \in Q^+$ the retarded single layer potential

$$\mathrm{SL}\, w(t,x) = \int_\Gamma \frac{w(t - \|x-y\|, y)}{4\pi \|x-y\|} \mathrm{d}S(y) \tag{4}$$

and the retarded double layer potential

$$\mathrm{DL}\, v(t,x) = \int_\Gamma \frac{\langle n(y), x-y \rangle}{4\pi \|x-y\|^2} \left(\frac{v(t - \|x-y\|, y)}{\|x-y\|} + \partial_t v(t - \|x-y\|, y) \right) \mathrm{d}S(y)$$

satisfy Eqs. (1) and (2) if the densities are extended such that $w(t,\cdot) = 0$ and $v(t,\cdot) = 0$ for $t < 0$, see e.g. [64]. Note that the name *retarded* is due to the property that these operators integrate their input densities along the retarded time $t - \|x-y\|$, which is elaborated in detail in Section 3. Applying the trace to the layer potentials induces the retarded single and double layer boundary integral operators

$$\gamma_0^+ \mathrm{SL} = \mathrm{V} \quad , \quad \gamma_0^+ \mathrm{DL} = \sigma \mathrm{I} + \mathrm{K}$$

where $\sigma : \Gamma \to \mathbb{R}$ is the solid angle or jump term defined by

$$\sigma(x) = \lim_{\varepsilon \to 0} \frac{1}{4\pi\varepsilon^2} \int_{y \in \Omega^- : \|x-y\| = \varepsilon} \mathrm{d}S(y), \quad x \in \Gamma.$$

For sufficiently smooth surface densities $w, v : \Sigma \to \mathbb{R}$ and $(t,x) \in \Sigma$ the retarded single and double layer boundary integral operators have the representations

$$\mathrm{V}\, w(t,x) = \int_\Gamma \frac{w(t-\|x-y\|,y)}{4\pi\|x-y\|} \mathrm{d}S(y) \tag{5}$$

and

$$\mathrm{K}\, v(t,x) = \int_\Gamma \frac{\langle n(y), x-y\rangle}{4\pi\|x-y\|^2} \left(\frac{v(t-\|x-y\|,y)}{\|x-y\|} + \partial_t v(t-\|x-y\|,y) \right) \mathrm{d}S(y)$$

as weakly singular surface integrals. Again, the densities are tacitly extended by zero for negative times in these integral representations. For solutions of Eqs. (1) and (2) the representation formula, also known as Kirchhoff's formula

$$u = \mathrm{DL}\, \gamma_0^+ u - \mathrm{SL}\, \gamma_1^+ u \tag{6}$$

holds. With Eq. (6) a solution of Eqs. (1) and (2) is unambiguously defined by its Cauchy data $(\gamma_0^+ u, \gamma_1^+ u)$ only. In this work, however, we shall not use Eq. (6) to construct solutions of the initial-boundary value problem but we pursue a slightly simpler approach. We employ the ansatz $u \coloneqq \mathrm{SL}\, w$ which satisfies Eqs. (1) and (2) for any suitable surface density w. To satisfy Eq. (3) the trace is applied to the ansatz yielding the boundary integral equation

$$\mathrm{V}\, w = g. \tag{7}$$

This method is an *indirect approach* since the surface density w is in general not related to a physical quantity. However, in certain transmission problems this density can indeed be identified with a physically meaningful quantity, cf. [64].

3 Space-time discretizations of RPBIEs

To obtain approximate solutions of the boundary integral equation Eq. (7) we develop in this chapter a space-time collocation approach. To this end, the lateral boundary Σ is decomposed into a mesh Σ_N of $N \in \mathbb{N}$ open boundary elements τ with

$$\Sigma_N = \{\tau_\ell\}_{\ell=1}^N, \quad \tau_i \cap \tau_j = \varnothing \text{ for } i \neq j, \quad \overline{\Sigma} = \bigcup_{\tau\in\Sigma_N} \overline{\tau}.$$

The explicit choice of the geometric shape of the boundary elements is detailed in Section 3.2. The local and global mesh size are defined by

$$h_\tau \coloneqq |\tau|^{1/3}, \quad h \coloneqq \max_{\tau\in\Sigma_N} h_\tau.$$

Each boundary element is the image of the same reference element $\hat{\tau}$ under a smooth bijective parametrization $\chi_\tau : \hat{\tau} \to \tau$. The gradient of the parametrization induces the Jacobi matrix

$$\mathbb{R}^{4\times 3} \ni J_\tau(\xi) \coloneqq \nabla\chi_\tau(\xi) = \begin{pmatrix} \partial_1\chi_\tau(\xi) & \partial_2\chi_\tau(\xi) & \partial_3\chi_\tau(\xi) \end{pmatrix}$$

whose columns are the three tangential vectors $\partial_i \chi_\tau(\xi), i = 1,2,3$. Since we assume that the parametrizations are regular, i.e. the boundary elements are non-degenerate, $\operatorname{rank} J_\tau(\xi) = 3$ holds for all $\xi \in \hat{\tau}$. Consequently, the matrix

$$\mathbb{R}^{3\times 3} \ni G_\tau(\xi) := J_\tau^\top(\xi) J_\tau(\xi) = \left(\left\langle \partial_i \chi_\tau(\xi), \partial_j \chi_\tau(\xi) \right\rangle\right)_{i,j=1}^3 .$$

is (symmetric) positive definite for all $\xi \in \hat{\tau}$. Note that $G_\tau(\xi)$ contains the covariant coefficients of the first fundamental form of Σ at $\chi_\tau(\xi)$. Another important quantity is the space-time normal vector field $\nu : \Sigma \to \mathbb{R}^4$. The normal vector is, by definition, orthogonal to the tangent vectors and consequently

$$\operatorname{span}\{\nu \circ \chi_\tau(\xi)\} = \ker J_\tau^\top(\xi)$$

holds. For stationary domains, as introduced in Section 2 it holds for $(t,x) \in \Sigma$

$$\nu(t,x) = \begin{pmatrix} \nu_t(t,x) \\ \nu_x(t,x) \end{pmatrix} = \begin{pmatrix} 0 \\ n(x) \end{pmatrix}$$

i.e. the time component ν_t is zero and the spatial component ν_x is just the normal vector of Γ.

To conclude this section, the employed trial spaces are discussed. In this work, standard finite element spaces, i.e. spaces of piecewise polynomial functions, on the mesh Σ_N are used. For simplicity we only consider the lowest-order trial spaces, namely the discontinuous trial space of piecewise constant functions

$$S_h^0(\Sigma_N) := \{v : \Sigma \to \mathbb{R} : v|_\tau \circ \chi_\tau \in \mathbb{P}^0(\hat{\tau}) \ \ \forall \tau \in \Sigma_N\}$$

and the continuous trial space of hat functions

$$S_h^1(\Sigma_N) := \{v : \Sigma \to \mathbb{R} : v|_\tau \circ \chi_\tau \in \mathbb{P}^1(\hat{\tau}) \ \ \forall \tau \in \Sigma_N\} \cap C(\Sigma).$$

These spaces are *space-time* trial spaces, since there is no inherent distinction between space and time coordinates. Within standard collocation approaches the unknown surface density is approximated by suitable ansatz functions and the boundary integral equation is interpolated at a set of collocation points. To fix ideas, consider the approximation $w_h \approx w$ of the solution of Eq. (7) where w_h is in one of the space-time trial spaces defined above. To collocate the boundary integral equation at $(t,x) \in \Sigma$ an evaluation of $\mathrm{V}\, w_h(t,x)$ is necessary. While integral representations of retarded potentials like Eqs. (4) and (5) are suitable for classical methods that discretize space and time separately, they are inconvenient for capturing the action of retarded potentials on space-time trial functions. To this end we derive a different representation of retarded potentials for the space-time mesh Σ_N in the following subsection.

3.1 Retarded potentials and space-time meshes

For convenience of notation we introduce an operator that unifies the integral representations of SL, DL, V, and K. For an arbitrary but fixed evaluation point $(t,x) \in [0,T] \times \mathbb{R}^3$ and surface density $w \in L^\infty(\Sigma)$ the abstract retarded potential integral operator T_k is defined by

$$\mathrm{T}_k\, w(t,x) = \int_\Gamma k(x,y) w(t - \|x-y\|, y) \mathrm{d}S(y) \tag{8}$$

where $k : \mathbb{R}^3 \times \mathbb{R}^3 \to \mathbb{R}$ denotes the kernel function and w is extended trivially for negative times. For the three kernel functions of interest

$$k_1(x,y) = \frac{1}{4\pi\|x-y\|}, \quad k_2(x,y) = \frac{\langle n(y), x-y\rangle}{4\pi\|x-y\|^3}, \quad k_3(x,y) = \frac{\langle n(y), x-y\rangle}{4\pi\|x-y\|^2} \tag{9}$$

the integral Eq. (8) exists as weakly singular surface integral if $(t,x) \in \Sigma$, see [62, Th. 3.3.5, Lem. 3.3.8]. The operator T_k is identified with the operators of Section 2 via

$$\mathrm{V} \leftrightarrow \mathrm{SL} = \mathrm{T}_{k_1}, \quad \mathrm{K} \leftrightarrow \mathrm{DL} = \mathrm{T}_{k_2} + \mathrm{T}_{k_3}\,\partial_t.$$

In order to recast Eq. (8) we introduce the function $\phi : \mathbb{R} \times \mathbb{R}^3 \to \mathbb{R}$

$$\phi(\zeta, y) = \|x-y\| - (t-\zeta)$$

whose zero level set

$$\Xi := \{(\zeta, y) \in \mathbb{R} \times \mathbb{R}^3 : \phi(\zeta, y) = 0\}$$

is a three-dimensional conical hypersurface embedded in four-dimensional space-time with apex at (t,x) and axis parallel to the time axis. This entity, which is known as the *backward light cone*, is the support of the causal fundamental solution of the wave equation, see [51, Op. 51] or [52, Ex. 1.4.12]. An illustration of the light cone in 2+1 dimensions is provided in Section 3.1.

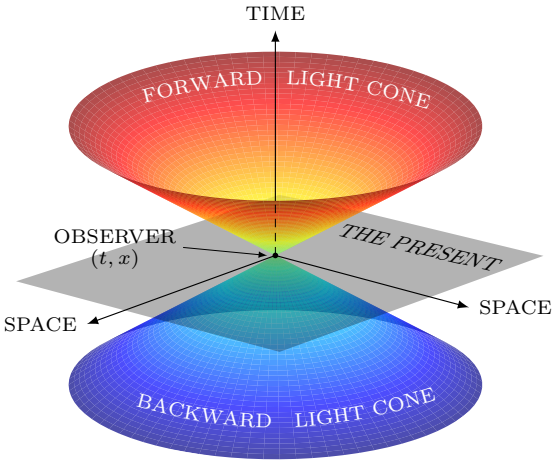

Figure 1: Visualization of the light cone at observation point (t,x) in $2+1$ dimensions. The observer at (t,x) perceives only signals emitted on the backward light cone. Conversely, a signal emitted at (t,x) is perceived only by observers located on the forward light cone. This idea bestows a physical interpretation to retarded potentials which integrate along the intersection of the backward light cone and the lateral boundary of the space-time cylinder, see Eq. (11b).

By using the Dirac delta δ_0 in a formal sense in conjunction with the decomposition Σ_N as

well as the parametrization of the boundary elements, Eq. (8) is rewritten

$$\begin{aligned}\mathrm{T}_k\, w(t,x) &= \int_\Gamma \int_0^T k(x,y) w(\zeta,y) \delta_0 \circ \phi(\zeta,y) \mathrm{d}\zeta \mathrm{d}S(y) \\ &= \sum_{\tau\in\Sigma_N} \int_{\hat{\tau}} k(x,\cdot) \circ |_x \chi_\tau(\xi) w \circ \chi_\tau(\xi) \delta_0 \circ \phi \circ \chi_\tau(\xi) \sqrt{\det G_\tau(\xi)} \mathrm{d}\xi\end{aligned}$$

where $|_x\chi_\tau(\xi)$ denotes the restriction of the vector $\chi_\tau(\xi)$ to the spatial component only. By introducing the integrand

$$f_\tau(\xi) = k(x,\cdot) \circ |_x \chi_\tau(\xi) w \circ \chi_\tau(\xi) \sqrt{\det G_\tau(\xi)}$$

we obtain

$$\mathrm{T}_k\, w(t,x) = \sum_{\tau\in\Sigma_N} \int_{\hat{\tau}} \delta_0 \circ \phi \circ \chi_\tau(\xi) f_\tau(\xi) \mathrm{d}\xi. \tag{10}$$

To endow this formal expression with a more intuitive interpretation, we shall use the coarea formula.

Theorem 3.1 (Coarea formula [19]). Let $\Omega \subset \mathbb{R}^d$, $d \geq 2$ be open, $f : \Omega \to \mathbb{R}$ be Lipschitz continuous and $g : \Omega \to \mathbb{R}$ be integrable. Then it holds

$$\int_\Omega g(x) \|\nabla f(x)\| \mathrm{d}x = \int_{\mathbb{R}} \left(\int_{x\in\Omega : f(x)=z} g(x) \mathrm{d}S(x) \right) \mathrm{d}z.$$

Formally applying the coarea formula to Eq. (10) yields the desired integral representation

$$\mathrm{T}_k\, w(t,x) = \sum_{\tau\in\Sigma_N} \int_{\mathbb{R}} \delta_0(z) \left(\int_{\xi\in\hat{\tau} : \phi\circ\chi_\tau(\xi)=z} \frac{f_\tau(\xi)}{\|\nabla(\phi\circ\chi_\tau(\xi))\|} \mathrm{d}S(\xi) \right) \mathrm{d}z \tag{11a}$$

$$= \sum_{\tau\in\Sigma_N} \int_{\chi_\tau^{-1}(\Xi\cap\tau)} k(x,\cdot) \circ |_x \chi_\tau(\xi)\, w \circ \chi_\tau(\xi) \frac{\sqrt{\det G_\tau(\xi)}}{\|\nabla(\phi\circ\chi_\tau(\xi))\|} \mathrm{d}S(\xi). \tag{11b}$$

where

$$\chi_\tau^{-1}(\Xi\cap\tau) = \{\xi \in \hat{\tau} : \phi \circ \chi_\tau(\xi) = 0\}$$

is the intersection of the backward light cone Ξ and the boundary element τ in terms of reference coordinates. Note that in order to apply Theorem 3.1 formally to Eq. (10) the function

$$\hat{\tau} \to \mathbb{R} : \ \xi \mapsto \frac{f_\tau(\xi)}{\|\nabla(\phi\circ\chi_\tau(\xi))\|}$$

has to be integrable. While f_τ is integrable by assumption, the following lemma captures an important property of the term $\nabla(\phi \circ \chi_\tau)$.

Lemma 3.1. For $\xi \in \hat{\tau}$ almost everywhere $\nabla(\phi \circ \chi_\tau(\xi)) = J_\tau^\top(\xi)\nabla\phi \circ \chi_\tau(\xi)$ and

$$\beta_2(\xi) \leq \|\nabla(\phi \circ \chi_\tau(\xi))\|^2 \leq 2\beta_4(\xi)$$

hold, where $0 = \beta_1(\xi) < \beta_2(\xi) \leq \beta_3(\xi) \leq \beta_4(\xi)$ are the eigenvalues of $J(\xi)J^\top(\xi)$.

The proof is only technical and carried out in Appendix A. By Lemma 3.1 the function $\|\nabla(\phi \circ \chi_\tau)\|$ is bounded from below (and above) by positive constants which implies

$$\frac{1}{\|\nabla(\phi \circ \chi_\tau)\|} \in L^\infty(\hat{\tau}).$$

It follows that the integrand in Eq. (11b) is integrable and the application of Theorem 3.1 to Eq. (10) is justified, at least in the claimed formal sense.

Representation Eq. (11b) strikingly shows that retarded layer potentials integrate over the intersection of the backward light cone Ξ and the lateral boundary Σ. Both Ξ and Σ are three-dimensional hypersurfaces embedded in $\mathbb{R}^4$, hence, their (non-empty, non-degenerate) intersection is a two-dimensional surface. The inverse of χ_τ expresses $\Xi \cap \tau$ in terms of the reference coordinates of the boundary element τ. Consequently $\chi_\tau^{-1}(\Xi \cap \tau)$ is a two-dimensional surface in three-dimensional parameter space. It is clear that the complexity of this surface is controlled by both the light cone Ξ as well as the boundary element τ. On the one hand the light cone is dictated by the wave equation itself, hence it is a fixed quantity. On the other hand there is some flexibility in the choice of the shape of the boundary elements. As already mentioned in the introduction, the goal of this paper is to take a first decisive step towards space-time boundary element methods for RPBIEs. In this context, we think it is justified to restrict ourselves to the simplest possible scenario for $\Xi \cap \tau$, i.e. choosing the simplest boundary elements. In the next subsection we discuss the chosen boundary elements.

3.2 Piecewise flat boundary description

As already mentioned, the lateral boundary Σ is a three-dimensional hypersurface embedded in $\mathbb{R}^4$. The simplest boundary elements are simplex type elements, which are in this case tetrahedral surface elements. Any tetrahedron τ can be parametrized by the affine map $\chi : \hat{\tau} \to \tau$

$$\chi : \xi \mapsto \begin{pmatrix} t_0 \\ x_0 \end{pmatrix} + J\xi \tag{12}$$

with the constant Jacobi matrix $J \in \mathbb{R}^{4\times 3}$ with $\operatorname{rank} J = 3$. Here $(t_0, x_0^\top)^\top$ is the coordinate vector of the first vertex of the tetrahedron τ. Furthermore, the space-time normal vector ν with $\operatorname{span}\{\nu\} = \ker J^\top$ is also constant. The Jacobi matrix has the block structure $J^\top = \begin{pmatrix} j_t & J_x^\top \end{pmatrix}$ where $j_t \in \mathbb{R}^3$ is the time component and $J_x \in \mathbb{R}^{3\times 3}$ is the spatial component. As already discussed, the time component of the space-time normal vector vanishes for stationary boundaries ($\nu_t = 0$). It follows

$$0 = J^\top \nu = j_t \nu_t + J_x^\top n = J_x^\top n$$

which implies $1 = \dim\ker J_x^\top = \dim\ker J_x$ since J_x is a square matrix. Obviously, Eq. (12) is well-defined in the entire reference space $\mathbb{R}^3$. This motivates to think of Eq. (12) as map

$\chi : \mathbb{R}^3 \to \operatorname{ran}\chi$ (ran denotes the range) and the parametrization of τ as the restriction $\chi|_{\hat{\tau}} : \hat{\tau} \to \tau$. From here on, χ shall always denote the extended affine map $\chi : \mathbb{R}^3 \to \operatorname{ran}\chi$. Its range $\operatorname{ran}\chi$ is a three-dimensional affine subspace of $\mathbb{R}^4$. In other words, $\operatorname{ran}\chi$ is the tangent hyperplane induced by the normal vector ν of the flat element τ.

At this point a brief comment about the construction of tetrahedral boundary meshes in $3+1$ dimensions is in order. To set up basis functions for the continuous trial space $S_h^1(\Sigma_N)$ in the standard way, the decomposition Σ_N has to be admissible. In the case of tetrahedral boundary elements the mesh is admissible iff the nonempty intersection $\overline{\tau}_i \cap \overline{\tau_j}$, $\tau_i \neq \tau_j \in \Sigma_N$ is either a common vertex, an edge, or a triangle. The construction of admissible space-time meshes is done as in [36]. In this article, the authors describe a procedure to construct admissible decompositions into simplex finite elements for $d+1$ dimensions, where $d \in \{1,2,3\}$. Their algorithm starts from a decomposition of the d-dimensional spatial domain into simplex finite elements, extrudes each element to a space-time hyperprism and decomposes it into $(d+1)$-simplices. In our case, we start with an admissible decomposition of Γ into triangles and apply the algorithm to obtain the tetrahedral mesh Σ_N. Different strategies for generating space-time meshes can be found in [9, 20]. In Section 3.2 an illustration of a space-time boundary element mesh of $\Sigma = (0,1) \times \partial\Omega^-$, $\Omega^- = \left(-\frac{1}{2}, \frac{1}{2}\right)^3$ is provided.

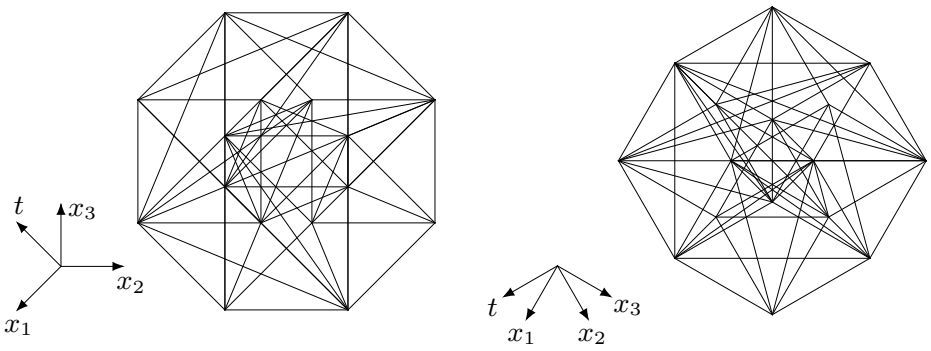

Figure 2: Wireframe depiction of a decomposition of $\Sigma = (0,1) \times \partial\Omega^-$ into 36 tetrahedrons, where Ω^- is the unit cube. Two different projections of the same mesh onto the two-dimensional canvas are illustrated. The projected base vectors of the Cartesian coordinate system in $3+1$ dimensional space-time are indicated by the arrows.

3.3 Intersection of light cone and flat boundary

Throughout the remainder of this section we consider a fixed but arbitrary evaluation point $(t,x) \in [0,T] \times \mathbb{R}^3$ and a tetrahedral boundary element $\tau \in \Sigma_N$ with affine parametrization $\chi : \mathbb{R}^3 \to \operatorname{ran}\chi$. For simplicity of notation we omit the subscripts related to τ and introduce the metric signature $M := \operatorname{diag}(-1,1,1,1)$. The surface in Eq. (11b) can be rewritten as

$$\chi^{-1}(\Xi \cap \tau) = \{\xi \in \mathbb{R}^3 : \phi_2 \circ \chi(\xi) = 0\} \cap \{\xi \in \mathbb{R}^3 : |_t\chi(\xi) \leq t\} \cap \hat{\tau} \tag{13}$$

where $|_t\chi(\xi)$ denotes the restriction of the vector $\chi(\xi)$ to its time component only and $\phi_2 : \mathbb{R}\times\mathbb{R}^3 \to \mathbb{R}$ is the quadratic level set function

$$\phi_2(\zeta, y) = \|x-y\|^2 - (t-\zeta)^2 = \left\langle M\begin{pmatrix} t-\zeta \\ x-y \end{pmatrix}, \begin{pmatrix} t-\zeta \\ x-y \end{pmatrix} \right\rangle .$$

In essence, Eq. (13) separates $\chi^{-1}(\Xi\cap\tau)$ into three components: The set $\{\xi : \phi_2\circ\chi(\xi) = 0\}$ is the intersection of the hyperplane $\operatorname{ran}\chi$ and the double light cone, i.e. both forward and backward portion, in terms of reference coordinates. The second part in Eq. (13) restricts to the backward light cone while the third part restricts to the actual boundary element. For now, we study the zero set of $\phi_2\circ\chi$, and recall that $\chi^{-1}(\Xi\cap\tau)$ is a certain subset of it.

For the sake of brevity, we denote the difference of the evaluation point and the first vertex of the tetrahedron

$$\mathbb{R}^4 \ni z_0 \coloneqq \begin{pmatrix} t-t_0 \\ x-x_0 \end{pmatrix}.$$

Insertion of the affine parametrization Eq. (12) yields the quadratic equation

$$\phi_2\circ\chi(\xi) = \langle A\xi,\xi\rangle + 2\langle b,\xi\rangle + c_0$$

with $A\in\mathbb{R}^{3\times3}$, $b\in\mathbb{R}^3$, and $c_0\in\mathbb{R}$ defined by

$$A \coloneqq J^\top MJ \quad , \quad b \coloneqq -J^\top Mz_0 \quad , \quad c_0 \coloneqq \langle Mz_0, z_0\rangle .$$

Since A is symmetric its eigenvalues are real and its eigenvectors form an orthonormal basis. Consequently, the quadratic equation can be simplified by principal axes transform, i.e. diagonalization of A. Let the ith column of $E\in\mathbb{R}^{3\times3}$ be the ith eigenvector of A associated to the eigenvalues $\lambda_1\le\lambda_2\le\lambda_3$. With the matrix $D \coloneqq \operatorname{diag}(\lambda_i)_{i=1}^3$ the diagonalization $A = EDE^\top$ is obtained. We introduce the affine map $\kappa : \mathbb{R}^3\to\mathbb{R}^3$

$$\kappa(\eta) = \xi_O + E\eta$$

with the origin $\xi_O = -A^{-1}b$ and get the quadratic equation in principal axes

$$\phi_2\circ\chi\circ\kappa(\eta) = \sum_{i=1}^3 \lambda_i\eta_i^2 + c_M \tag{14}$$

where $c_M \coloneqq \langle b,\xi_O\rangle + c_0$. Obviously ξ_O is well-defined iff A is invertible. The following lemma enables a categorization of Eq. (14).

Lemma 3.2. It holds $\lambda_1 < 0 < \lambda_2 \le \lambda_3$ and $c_M = \langle z_0,\nu\rangle^2 = \langle x-x_0,n\rangle^2$.

The proof of this lemma is merely technical and deferred to Appendix A. From Lemma 3.2 we observe that $c_M = 0$ iff $\langle z_0,\nu\rangle = 0$. This is the case iff $(t,x)\in\operatorname{ran}\chi$, i.e. the hyperplane induced by χ goes through the apex of the light cone at (t,x). From Lemma 3.2 it follows that the zero set of Eq. (14) and hence $\{\xi : \phi_2\circ\chi(\xi) = 0\}$ is an elliptic hyperboloid of two sheets if $(t,x)\notin\operatorname{ran}\chi$ or an elliptic double cone if $(t,x)\in\operatorname{ran}\chi$. One sheet of the hyperboloid or one

cone of the double cone is associated to the forward light cone and consequently not of interest for Eq. (13). The eigenvector e_1 with eigenvalue $\lambda_1 < 0$ is oriented such that

$$\langle e_1, j_t \rangle < 0 \tag{15}$$

where we recall that j_t is the first column of $J^\top$. This condition ensures that a coordinate with $\eta_1 > 0$ is associated to the backward light cone while $\eta_1 < 0$ is related to the forward light cone.

As next step Eq. (11b) is transformed to an integral in a parameter domain of the light cone in reference coordinates. The employed parametrization is available for flat boundary elements as discussed previously. The integral in Eq. (11b) is abbreviated

$$\mathscr{I} := \int\limits_{\chi^{-1}(\Xi \cap \tau)} k_x(\xi) w_{\hat{\tau}}(\xi) \mathrm{d}S(\xi) \tag{16}$$

where

$$k_x(\xi) = k(x,\cdot) \circ |_x \chi(\xi), \quad w_{\hat{\tau}}(\xi) = w \circ \chi(\xi) \frac{\sqrt{\det G}}{\|\nabla(\phi \circ \chi(\xi))\|}, \quad \xi \in \hat{\tau}.$$

As already discussed, Lemma 3.2 implies that $\chi^{-1}(\Xi \cap \tau)$ is a subset of either a cone or a sheet of a two-sheeted hyperboloid. The key ingredients of the employed transformation are well-known parametrizations of the cone/hyperboloid. The backward cone is parametrized by

$$\begin{aligned} \psi_C : [0,2\pi) \times [0,\infty) &\to \mathbb{R}^3 \\ \begin{pmatrix} \rho_1 \\ \rho_2 \end{pmatrix} &\mapsto \rho_2 \begin{pmatrix} 1 \\ \alpha_2 \cos\rho_1 \\ \alpha_3 \sin\rho_1 \end{pmatrix} \end{aligned}$$

with $\alpha_i := \sqrt{-\lambda_1/\lambda_i}$ for $i = 2,3$. The backward sheet of the two-sheeted hyperboloid is parametrized by

$$\begin{aligned} \psi_H : [0,2\pi) \times [0,\infty) &\to \mathbb{R}^3 \\ \begin{pmatrix} \rho_1 \\ \rho_2 \end{pmatrix} &\mapsto \begin{pmatrix} \alpha_1 \cosh\rho_2 \\ \alpha_2 \sinh\rho_2 \cos\rho_1 \\ \alpha_3 \sinh\rho_2 \sin\rho_1 \end{pmatrix} \end{aligned}$$

with $\alpha_i := \sqrt{c_M/|\lambda_i|}$ for $i = 1,2,3$. The desired parametrization is defined by

$$\psi := \begin{cases} \kappa \circ \psi_C & c_M = 0 \\ \kappa \circ \psi_H & c_M > 0 \end{cases}$$

where Eq. (15) ensures that ψ maps onto the backward portion of the light cone only. We introduce $\operatorname{dom}\psi := [0,2\pi) \times [0,\infty)$ (dom denotes the domain) and by construction $\operatorname{ran}\psi = \chi^{-1}(\Xi \cap \operatorname{ran}\chi)$ holds. This allows us to carry the integral Eq. (16) over to an integral in $\operatorname{dom}\psi$. However, since Eq. (16) integrates along $\chi^{-1}(\Xi \cap \tau) = \operatorname{ran}\psi \cap \hat{\tau}$ the integral is posed on the subset

$$\Theta := \{\rho \in \operatorname{dom}\psi : \psi(\rho) \in \hat{\tau}\} = \psi^{-1}(\hat{\tau} \cap \operatorname{ran}\psi).$$

In this context we use the notation ψ^{-1} in a formal sense, since ψ is not injective on $\operatorname{dom}\psi$ but only on the dense subset $[0,2\pi)\times(0,\infty)$. This is due to the fact that ψ maps the entire line $[0,2\pi)\times\{0\}$ to the vertex of the cone/hyperboloid. We obtain

$$\mathscr{I} = \int_{\Theta} k_x \circ \psi(\rho) w_{\hat{\tau}} \circ \psi(\rho) g_\psi(\rho) \mathrm{d}\rho \tag{17}$$

with the transformation determinant

$$g_\psi(\rho) = \left(\det\left(\left\langle \partial_i \psi(\rho), \partial_j \psi(\rho) \right\rangle \right)_{i,j=1}^{2} \right)^{1/2}.$$

This parametrization of the light cone in reference coordinates is depicted in Section 3.3.

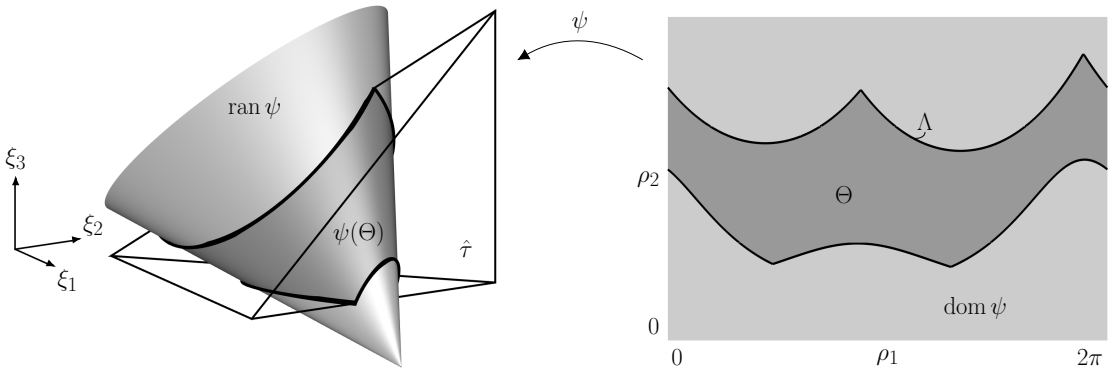

Figure 3: Sketch of the parametrization of the light cone in reference coordinates of a tetrahedral boundary element.

Our goal is to employ numerical integration based on Gaussian quadrature rules to approximate Eq. (17). Representation Eq. (17) is advantageous for this purpose, since the product of kernel function and transformation determinant defines a smooth function.

Lemma 3.3. For any $\rho \in \operatorname{dom}\psi$ it holds

$$g_\psi(\rho) = \begin{cases} -\lambda_1 \rho_2 g_C(\rho) & c_M = 0 \\ c_M \sinh\rho_2 \cosh\rho_2 g_H(\rho) & c_M > 0 \end{cases}$$

where $g_C, g_H : \operatorname{dom}\psi \to \mathbb{R}$ are smooth and $0 < (\lambda_2\lambda_3)^{-1/2} \leq g_H(\rho) < g_C(\rho)$. Moreover, let $d_x(y) = \|x-y\|$ for any $x,y \in \mathbb{R}^3$. For any $\rho \in \operatorname{dom}\psi$

$$d_x \circ |_x\chi \circ \psi(\rho) = \begin{cases} \sqrt{-\lambda_1}\rho_2 f_C(\rho) & c_M = 0 \\ \sqrt{c_M}\cosh\rho_2 f_H(\rho) & c_M > 0 \end{cases}$$

where $f_C, f_H : \operatorname{dom}\psi \to \mathbb{R}$ are smooth and bounded from below by a positive constant.

The proof is given in Appendix A.

Theorem 3.2. Let $k_i, i = 1,2,3$ be the functions as in Eq. (9). For any $x \in \mathbb{R}^3$ the function $k_i^*(\rho) = k_i(x,\cdot)\circ|_x\chi \circ \psi(\rho) g_\psi(\rho)$ can be extended to $C^\infty(\mathbb{R}\times[0,\infty))$.

Proof. As discussed in Section 3.2 it holds $J_x^\top n = 0$. From Lemma 3.2 we have $c_M = \langle n, x - x_0\rangle^2$ and for any $\xi \in \mathbb{R}^3$

$$\langle n, x - |_x\chi(\xi)\rangle^2 = \langle n, x - x_0 - J_x\xi\rangle^2 = \langle n, x - x_0\rangle^2 = c_M$$

follows. For any $\rho \in \mathbb{R}\times[0,\infty)$ the map ψ is well-defined and takes values in $\operatorname{ran}\psi$ due to periodicity in the first component. Consider the functions $k_i^* : \mathbb{R}\times[0,\infty) \to \mathbb{R}$ defined by $k_i^* : \rho \mapsto k_i(x,\cdot)\circ|_x\chi\circ\psi(\rho)g_\psi(\rho)$, where $k_i, i = 1,2,3$ is as in Eq. (9) apart from the division by 4π. There hold the representations for $c_M = 0$

$$k_1^*(\rho) = \sqrt{-\lambda_1}\frac{g_C(\rho)}{f_C(\rho)},\ k_2^*(\rho) = 0,\ k_3^*(\rho) = 0$$

and for $c_M > 0$ with $s_x := \operatorname{sgn}\langle n, x - x^0\rangle \neq 0$

$$k_1^*(\rho) = \sqrt{c_M}\sinh\rho_1\frac{g_H(\rho)}{f_H(\rho)},\ k_2^*(\rho) = s_x\frac{\tanh\rho_1}{\cosh\rho_1}\frac{g_H(\rho)}{f_H^3(\rho)},\ k_3^*(\rho) = s_x\sqrt{c_M}\tanh\rho_1\frac{g_H(\rho)}{f_H^2(\rho)}$$

with f_X, g_X for $X \in \{C,H\}$ as in Lemma 3.3. The smoothness of above functions is an immediate consequence of Lemma 3.3 which concludes the proof. □

Theorem 3.2 conveys that the transformation induced by ψ regularizes the potentially weakly singular integral Eq. (16), which is a decisive advantage of representation Eq. (17). To enable the application of existing numerical integration techniques, we recast Θ to an implicitly defined set. To this end, consider a continuous function $\phi_{\hat\tau} : \mathbb{R}^3 \to \mathbb{R}$ such that

$$\phi_{\hat\tau}(\xi)\begin{cases} < 0 & \xi \in \hat\tau \\ = 0 & \xi \in \partial\hat\tau \\ > 0 & \text{otherwise} \end{cases}.$$

Since the reference tetrahedron $\hat\tau$ is the intersection of four open half spaces the function $\phi_{\hat\tau}$ can be defined by

$$\phi_{\hat\tau}(\xi) = \max_{i=1,\dots,4}\{d_i(\xi)\}$$

where $d_i : \mathbb{R}^3 \to \mathbb{R}$ for $i = 1,\dots,4$ is the signed distance function of the plane that defines the ith half space. This allows the equivalent definition

$$\Theta = \{\rho \in \operatorname{dom}\psi : \phi_{\hat\tau}\circ\psi(\rho) < 0\}. \tag{18}$$

There exist several methods for computing approximations of the integral Eq. (17) with the implicitly defined set Eq. (18). Common approaches are based on (high-order) approximations or reconstructions of the implicitly defined set [37, 22, 23]. A prominent alternative uses the divergence theorem in conjunction with a moment-fitting method to avoid such reconstructions

to the geometry [48]. Another interesting technique is based on local parametrizations due to the implicit function theorem [65]. We conjecture that all of these procedures yield reliable results for Eq. (17). Nevertheless, we shall provide an alternative approach tailored to the situation at hand.

Remark 1. Although this work deals with stationary boundaries only, several results can indeed be generalized to instationary ones. The main assumption within this generalization is that the normal velocity of the boundary element is lower than the speed of wave propagation (which is 1 due to the scaled time coordinate). In this case, there is also a positive constant that bounds $\|\nabla(\phi \circ \chi_\tau)\|^2$ from below, similar to Lemma 3.1. Moreover, the signs of the eigenvalues and the sign of c_M in Lemma 3.2 remain valid. This implies that the hyperconic section $\Xi \cap \operatorname{ran} \chi$ remains a cone/hyperboloid as long as the simplex boundary element travels below wave speed. We emphasize that we do not provide these results here, as the focus of this paper lies on the space-time methodology itself rather than instationary domains.

3.4 A quadrature scheme for $\mathscr{I}$

In the following paragraphs a numerical integration technique for evaluating Eq. (17) is devised. The integral $\mathscr{I}$ is recast into a sum of integrals over a simple reference interval, which are treated by standard Gaussian quadrature. For ease of notation we abbreviate the integrand

$$k_\psi(\rho) = k_x \circ \psi(\rho) w_{\hat{\tau}} \circ \psi(\rho) g_\psi(\rho), \quad \rho \in \Theta$$

and introduce the integrated kernel

$$k_\psi^+(\rho_1, \rho_2) = \int_0^{\rho_2} k_\psi(\rho_1, r) \mathrm{d}r = \rho_2 \int_0^1 k_\psi(\rho_1, \rho_2 r) \mathrm{d}r, \quad (\rho_1, \rho_2) \in \overline{\Theta}. \tag{19}$$

Note that Eq. (19) is well-defined only if there exists a suitable extension of k_ψ outside of Θ. By Theorem 3.2, the product of $k_x \circ \psi$ and g_ψ defines a smooth function in $\operatorname{dom} \psi$. A straightforward computation shows that $\nabla(\phi \circ \chi_\tau) \circ \psi$ does also induce a smooth function in $\operatorname{dom} \psi$ and in conjunction with Lemma 3.1 it follows that the reciprocal of $\|\nabla(\phi \circ \chi_\tau) \circ \psi\|$ is a smooth function in $\operatorname{dom} \psi$ as well. Consequently, the only term that might cause difficulties is the density function w, for which an extension to a sufficiently large (tangential) neighbourhood around τ has to exist. However, in practical computations $w|_\tau \circ \chi$ is a polynomial basis function, for which the extension to an entire function is obvious. Hence, we may assume that Eq. (19) is well-defined and its integrand is smooth.

As a consequence, we can apply the divergence theorem, also known as the Gauss-Ostrogradsky theorem, which yields

$$\mathscr{I} = \int_{\partial\Theta} k_\psi^+(\rho) n_2^\Theta(\rho) \mathrm{d}S(\rho) = \int_\Lambda k_\psi^+(\rho) n_2^\Theta(\rho) \mathrm{d}S(\rho) \tag{20}$$

where n_2^Θ denotes the ρ_2-component of the unit outward normal vector field to Θ and

$$\Lambda := \{\rho \in \operatorname{dom} \psi : \phi_{\hat{\tau}} \circ \psi(\rho) = 0\} = \psi^{-1}(\partial\hat{\tau} \cap \operatorname{ran} \psi) \subseteq \partial\Theta.$$

Although Λ can be a subset of $\partial\Theta$, the second equality in Eq. (20) holds since integrals on $\{0,2\pi\}\times[0,\infty)$ and $[0,2\pi)\times\{0\}$ vanish, as either n_2^Θ or k_ψ^+ vanishes. In a certain sense, Eq. (20) reduces $\mathscr{I}$ to an integral along the curve Λ, as only a parametrization of Λ is necessary to enable the application of standard quadrature schemes. We employ piecewise smooth parametrizations as discussed in [38], a closely related approach is proposed in [25]. The technique is reiterated here for the sake of completeness. Assume that we are given a piecewise affine interpolation Λ_1 of Λ, i.e. Λ_1 is a collection of line elements σ whose end points lie on Λ. Each line $\sigma\in\Lambda_1$ is defined by its two end points $\rho_\sigma^A,\rho_\sigma^B\in\Lambda$ and parametrized by $\ell_\sigma:(0,1)\to\sigma$ with $\ell_\sigma(r)=\rho_\sigma^A+(\rho_\sigma^B-\rho_\sigma^A)r$. We introduce the strip around Λ of width $\varepsilon>0$

$$\Theta_\varepsilon := \{\rho\in\operatorname{dom}\psi : \operatorname{dist}(\rho,\Lambda)\le\varepsilon\}.$$

As in [38] we consider the transformation $\iota:\Theta_\varepsilon\to\Lambda$ defined by

$$\iota(\rho)=\rho+d(\rho)s(\rho) \tag{21}$$

with search direction field $s:\Theta_\varepsilon\to\mathbb{R}^2$ and the the distance function $d:\Theta_\varepsilon\to\mathbb{R}$. We use $s(\rho)=\nabla(\phi_{\hat\tau}\circ\psi(\rho))$ and $d(\rho)$ is the solution with smallest absolute value of

$$d(\rho)\in\mathbb{R}: \quad \phi_{\hat\tau}\circ\psi(\rho+d(\rho)s(\rho))=0, \quad \rho\in\Theta_\varepsilon. \tag{22}$$

This transformation mimics the closest point projection, cf. [16, 25]. A parametrization of a subset of Λ is obtained by $\iota_\sigma := \iota\circ\ell_\sigma$ for $\sigma\in\Lambda_1$. It is important to note that Eq. (21) is well-defined only if ε is sufficiently small. To ensure that the line σ lies in Θ_ε it has to be sufficiently close to Λ, which implies that Λ_1 has to be sufficiently close to Λ. The construction of Λ_1 is discussed in Appendix B. Here, we assume that ι_σ is injective for all $\sigma\in\Lambda_1$ and

$$\overline{\Lambda}=\bigcup_{\sigma\in\Lambda_1}\overline{\operatorname{ran}\iota_\sigma} \quad\wedge\quad \operatorname{ran}\iota_\sigma\cap\operatorname{ran}\iota_\mu=\varnothing,\sigma\neq\mu\in\Lambda_1$$

giving rise to the transformed integral

$$\mathscr{I}=\sum_{\sigma\in\Lambda_1}\int_0^1 k_\psi^+\circ\iota_\sigma(r)n_2^\Theta\circ\iota_\sigma(r)\|\iota_\sigma'(r)\|\,\mathrm{d}r. \tag{23}$$

By Eqs. (19) and (23) the evaluation of Eq. (17) is performed only by computation of integrals in the interval $(0,1)$. The integrands are smooth if ι_σ is smooth and we suggest to approximate the integral by Gaussian quadrature rules. Notice that the integrand in Eq. (19) is (in general) not analytic everywhere. Although this lack of analyticity prevents Gaussian quadrature schemes from reaching their optimal convergence properties, they still yield acceptable approximations. To conclude the discussion of the numerical computation of Eq. (16) we utter several remarks on the implementation of the proposed scheme:

- To approximate the integrals Eqs. (19) and (23) we employ standard Gauss-Legendre quadrature rules with $n_G\in\mathbb{N}$ integration points. There is potential for significant improvement, e.g. adaptive quadrature schemes could be applied, cf. [54].

- The choice of Eq. (19) is not unique. Alternatively, the kernel

$$\int_0^{\rho_1} k_\psi(r,\rho_2)\mathrm{d}r$$

in conjunction with the ρ_1-component of the unit outward normal field in Eqs. (20) and (23) could be used. In our implementation we opt for the kernel Eq. (19) as it yielded smaller quadrature errors in a few numerical experiments.

- The interval of integration $(0,\rho_2)$ in Eq. (19) can be improved. It seems reasonable to choose a lower bound $\rho_2^{\min} \geq 0$ such that the intervals $(\rho_2^{\min},\rho_2)$ are kept relatively small for any $\rho \in \Lambda$. This improves the error estimate of the Gaussian quadrature for the kernel k_ψ^+. However, if $\rho \in [0,2\pi) \times \{0\}$ satisfies $\phi_{\hat{\tau}} \circ \psi(\rho) \leq 0$, i.e. the apex of the cone/hyperboloid is in the closure of $\hat{\tau}$, we suggest to set $\rho_2^{\min} = 0$. Otherwise Eq. (20) might not reduce to Λ alone but a term along $[0,2\pi) \times \{0\}$ remains.

- The number $d(r)$ at $r \in (0,1)$ is a solution of the non-linear equation Eq. (22). To approximate this value Newton's method is employed [38, 25, 54]. Since we use the initial guess $d(\rho) = 0$ the convergence of this procedure relies heavily on the proximity of the line $\sigma \in \Lambda_1$ to Λ. This circumstance does not seem to pose a severe problem, as Λ_1 has to be sufficiently close to Λ to ensure that Eq. (21) is a well-defined anyway. In the examples reported in Section 4 at most 10 iterations in Newton's method were necessary to satisfy Eq. (22) up to machine precision.

3.5 Collocation method

To set up collocation equations of Eq. (7) an explicit choice of collocation points has to be made. In this work, we apply usual choices of collocation points well-established in boundary element methods for elliptic problems. For approximations $w_h \in S_h^0(\Sigma_N)$ the centroids of the elements are chosen as collocation nodes. The set of centroids of all elements of the mesh Σ_N is denoted $\mathscr{C}(\Sigma_N)$. This leads to the discretized boundary integral equation

$$w_h \in S_h^0(\Sigma_N) : \mathrm{V}\, w_h(t,x) = g(t,x), \quad (t,x) \in \mathscr{C}(\Sigma_N). \tag{24}$$

A problem somewhat similar to Eq. (24) is analyzed by Davies and Duncan [12]. In the cited paper, it is assumed that Γ is flat and the employed trial functions are products of functions in the spatial coordinates and functions in the time variable. The authors prove convergence of the solution of the arising collocation equations for certain trial spaces. However, they indicate that piecewise constant spatial basis functions yield unstable methods for a variety of mesh ratios. Since the trial functions in our approach are either continuous or discontinuous in space-time, we shall also consider approximations in $S_h^1(\Sigma_N)$. For $w_h \in S_h^1(\Sigma_N)$ the vertices of the tetrahedral mesh are chosen as collocation points. We denote the set of all vertices of Σ_N by $\mathscr{V}(\Sigma_N)$. For continuous solutions of Eqs. (1) to (3) the Dirichlet data g has to be compatible with the initial data, in particular the compatibility condition $g = 0$ on $\{0\} \times \Gamma$ has to hold. If the continuous

density w_h can be continuously extended by zero for negative times it follows $w_h = 0$ on $\{0\} \times \Gamma$. Consequently, we introduce the subspace

$$S^1_{h,0}(\Sigma_N) \coloneqq \{v \in S^1_h(\Sigma_N) : v = 0 \text{ on } \{0\} \times \Gamma\}$$

and the subset of vertices which serve as collocation points

$$\mathscr{V}_0(\Sigma_N) \coloneqq \{(t,x) \in \mathscr{V}(\Sigma_N) : t > 0\}.$$

This yields a discretization of Eq. (7) based on continuous basis functions

$$w_h \in S^1_{h,0}(\Sigma_N) : \mathrm{V}\, w_h(t,x) = g(t,x), \quad (t,x) \in \mathscr{V}_0(\Sigma_N). \tag{25}$$

To implement these boundary element discretizations, point-wise evaluations of retarded layer operators acting on space-time trial functions are required. On the one hand, evaluations $\mathrm{V}\, w_h(t,x)$ for $(t,x) \in \Sigma$ are necessary to set up the left hand sides in Eqs. (24) and (25). On the other hand, once the solution of Eq. (24) or Eq. (25) is computed, approximate solutions of Eqs. (1) to (3) are obtained by evaluating the ansatz $\mathrm{SL}\, w_h(t,x)$ for $(t,x) \in Q^+$. Both of these evaluations are realized by means of the numerical integration scheme introduced in Section 3.4.

4 Numerical experiments

In this section, the proposed method is verified by investigating elementary examples. In particular, the performance of the numerical integration technique as well as the overall space-time scheme is examined. To this end, we construct a simple, yet smooth solution of the wave equation. Consider a fixed source point $y_S \in \Omega^-$ and a sufficiently smooth signal $\mu : \mathbb{R} \to \mathbb{R}$ with $\operatorname{supp} \mu \subset [0,\infty)$. Then the spherical wave function $f : \mathbb{R} \times \{\mathbb{R}^3 \setminus y_S\} \to \mathbb{R}$

$$f(t,x) = \frac{\mu(t - \|x - y_S\|)}{\|x - y_S\|}$$

satisfies the wave equation subject to homogeneous initial conditions everywhere in its domain. Consequently, the restriction $u \coloneqq f|_{Q^+}$ defines a solution of Eqs. (1) and (2). The Dirichlet trace of this manufactured solution is the restriction $g = \gamma_0^+ u = f|_\Sigma$ and the Neumann trace is the normal derivative $\gamma_1^+ u = \langle n, (\nabla_x f)|_\Sigma \rangle$. We consider

$$\mu(s) = \begin{cases} \exp\left(\left(\frac{s^2}{4} - s\right)^{-1}\right) & s \in (0,4) \\ 0 & \text{otherwise} \end{cases}$$

which satisfies $\mu \in C^\infty(\mathbb{R})$. In all tests we use the source point $y_S = -(\frac{1}{10}, \frac{2}{10}, \frac{3}{10})^\top$, which is suitable for all examined scenarios.

4.1 Experiment 1: Verification of the quadrature technique

The first test is intended to verify the numerical integration procedure for retarded potentials. As computational domain we consider the unit cube $\Omega^- = \left(-\frac{1}{2},\frac{1}{2}\right)^3$ with $T = 5$. Our goal is to evaluate the expression

$$\widetilde{u}(t,x) := \begin{cases} \widetilde{\mathrm{DL}}\gamma_0^+ u(t,x) - \widetilde{\mathrm{SL}}\gamma_1^+ u(t,x) & (t,x) \in Q^+ \\ \sigma(x)\gamma_0^+ u(t,x) + \widetilde{\mathrm{K}}\gamma_0^+ u(t,x) - \widetilde{\mathrm{V}}\gamma_1^+ u(t,x) & (t,x) \in \Sigma \end{cases} \tag{26}$$

which is Kirchhoff's formula Eq. (6) for $(t,x) \in Q^+$ or its trace for $(t,x) \in \Sigma$. The tildes over the integral operators should indicate that they are approximated by numerical integration. Since a mesh is necessary to run the integration algorithm we employ a globally quasi uniform decomposition of Σ into 288 tetrahedrons. However, the *exact* Cauchy data $(\gamma_0^+ u, \gamma_1^+ u)$ are used in Eq. (26) rather than mere approximations of them in some finite element space defined on the mesh. The fact that we input the exact Cauchy data into the representation formula implies that the use of a mesh does not constitute an approximation. The only approximation is due to the numerical integration in the retarded potentials by an order $n_G \in \mathbb{N}$ quadrature scheme as devised in Section 3.4. The error is measured by computing

$$e_n = \frac{|u(T,x) - \widetilde{u}(T,x)|}{|u(T,x)|}$$

at the sampling point

$$x := \left(\tfrac{1}{2},\tfrac{1}{2},\tfrac{1}{2}\right)^\top + r\,(1,0,0)^\top$$

where $0 \le r = \operatorname{dist}(x,\Gamma)$. The results for different values of r are depicted in Section 4.1. It can be observed that the quadrature error decays rapidly as the number of integration points is increased. Convergence ceases at $e_n \approx 10^{-14}$ since this value is already quite close to the employed machine precision. Furthermore, there is little dependence on the distance of the evaluation point to the boundary. In particular, the case $r = 0$, in which integral operators with weakly singular kernels are evaluated, is handled as well as the cases with positive distance. This is due to the parametrization introduced in Section 3.3, which regularizes the integrand, see Theorem 3.2. We note that the stated observations are quite comparable to numerical results provided in the literature. In [61, Fig. 3.3] an integral with smooth (but not analytic) kernel, which arises in a Galerkin discretization of RPBIEs, is approximated by Gaussian quadrature. The quadrature errors observed in the cited reference feature a similar behaviour to our experiment.

We consider a further example to support the viability of the developed quadrature scheme for weakly singular kernel functions. Again Eq. (26) is evaluated, however, evaluation points exclusively *on* the boundary are of interest in this test. We study the two scenarios:

- *Cube:* In the first test we set $\Omega^- = \left(-\frac{1}{2},\frac{1}{2}\right)^3$ with $T = 5$, decomposed into a mesh of 288 elements ($h \approx 0.4705$). As a measure of error the arithmetic mean of the relative error of point evaluations on the vertices of the mesh

$$e_n^\Sigma = \frac{1}{50} \sum_{\substack{(t,x)\in\mathscr{V}(\Sigma_N):\\ |u(t,x)|>10^{-5}}} \frac{|u(t,x) - \widetilde{u}(t,x)|}{|u(t,x)|}$$

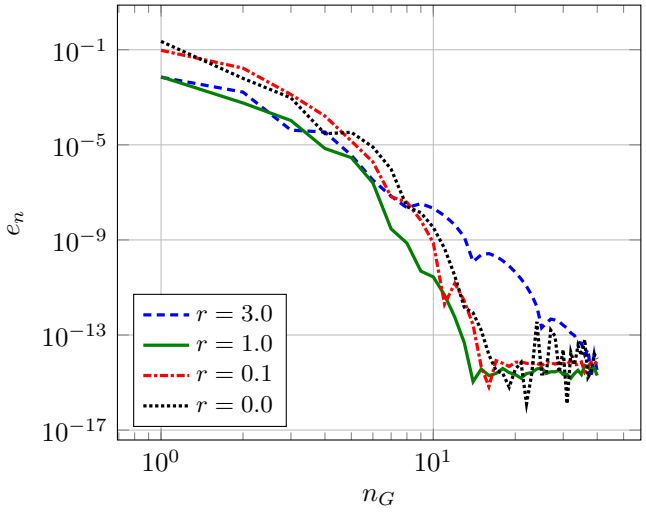

Figure 4: Convergence of the quadrature scheme for Kirchhoff's formula ($r > 0$) or its trace (weakly singular boundary integral equation, $r = 0$) respectively.

is used, where 50 is the number of vertices where $|u| > 10^{-5}$ holds. We set this threshold to prevent round-off errors from spoiling the observable convergence of the relative error.

- *Sphere:* In the second test $\Omega^- \approx \{x \in \mathbb{R}^3 : \|x\| < 1\}$ with $T = 2$ is considered. The employed mesh consisting of 2196 elements ($h \approx 0.2335$) does not represent an exact sphere, but a polyhedral approximation of it. We use a similar error measure as in the first test, but the evaluations are performed at the centroids of the elements

$$e_n^{\Sigma} = \frac{1}{988} \sum_{\substack{(t,x)\in\mathscr{C}(\Sigma_N):\\ |u(t,x)|>10^{-5}}} \frac{|u(t,x) - \widetilde{u}(t,x)|}{|u(t,x)|}$$

with 988 being the number of centroids where $|u| > 10^{-5}$ holds.

In Section 4.1, the result of this experiment is exhibited. Again, one can recognize that the error decays swiftly, especially in the pre-asymptotic regime. As expected by the lack of analyticity of the integrand, the error does however not decay at an exponential rate, cf. [61]. The error in the case of the sphere is smaller than in the case of the cube (roughly by some constant value). This is due to the fact, that the mesh size of the spherical mesh is substantially smaller, hence altogether more integration points (for the same value of n_G) are used to compute the integral operators along the lateral boundary Σ.

From these observations we conclude that the proposed numerical integration technique is indeed capable in computing reasonable approximations of point evaluations of retarded potential integral operators in the context of space-time meshes composed of simplex elements.

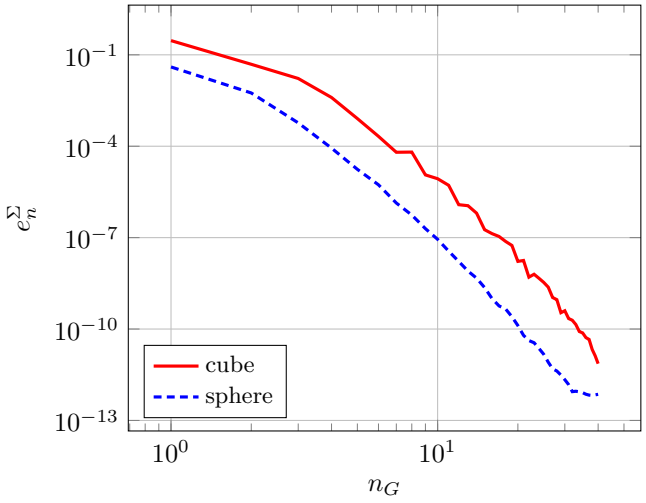

Figure 5: Convergence of the quadrature scheme for the weakly singular boundary integral equation.

4.2 Experiment 2: Collocation scheme

In this experiment the actual space-time collocation methods Eqs. (24) and (25) are tested. As in the previous example we set $\Omega^- = (-\frac{1}{2}, \frac{1}{2})^3$. We consider $T = 2$ as well as $T = 4$ to study the effect of the simulation end time. The used meshes are uniform and the integration order is fixed to $n_G = 10$. To measure the error, the difference of u and the ansatz $\mathrm{SL}\, w_h$ is examined, where w_h is the solution of Eq. (24) or Eq. (25). In particular, the arithmetic mean of 26 points $x \in \Omega^+$ spaced equally on the boundary of the cube $(-\frac{3}{5}, \frac{3}{5})^3$

$$e_n^Q = \frac{1}{26} \sum_{i=1}^{26} \frac{\left| u(T, x_i) - \widetilde{\mathrm{SL}} w_h(T, x_i) \right|}{|u(T, x_i)|}$$

is used to quantify the error. The convergence studies are depicted in Section 4.2.

It can be observed that for $T = 2$ the error e_n^Q decays roughly at first-order rate in the mesh size h within both approaches Eqs. (24) and (25). However, for $T = 4$ these methods fail to converge at all. This is an indication that these methods are not stable for arbitrary values of T. It is well-known that certain bilinear forms of RPBIEs are positive definite if the simulation end time is sufficiently small, see [35]. Notice that both $T = 2$ and $T = 4$ violate the criterion sufficient for positive definiteness stated in [35, Prop. 3.4.]. Nevertheless the "naive" collocation approaches Eqs. (24) and (25) are expected to tend more towards instability than the variational formulations employed in the cited reference. To the best of our knowledge, no theoretical results for collocation methods for RPBIEs on polyhedral boundaries are available (in particular in the context of space-time trial functions as used in this work). That is why, we endow the following interpretation to the numerical findings exhibited in this experiment: Discretization schemes for RPBIEs based on unstructured space-time meshes are technically feasible and the obtained numerical results indicate their great potential. Having said that, the discussed space-time collocation methods appear to have similar stability issues as classical approaches. The

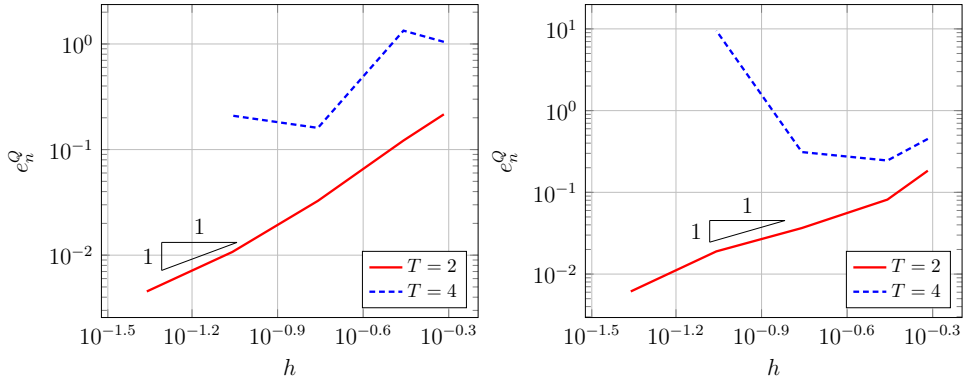

(a) method Eq. (24) based on S_h^0 (b) method Eq. (25) based on S_h^1

Figure 6: Convergence of the collocation methods for a sequence of uniform meshes, $\Omega^- = (-\frac{1}{2}, \frac{1}{2})^3$.

success of the space-time methodology vitally hinges on finding stable formulations in general settings.

5 Concluding remarks

In this paper, a space-time boundary element method for the wave equation in $3+1$ dimensions is proposed. Its key feature are basis functions that do not distinguish between space and time coordinates but are based on unstructured meshes of the lateral boundary of the space-time cylinder. An explicit representation of retarded potential integral operators appropriate for these basis functions is derived and a numerical integration scheme is developed. Numerical experiments confirm that space-time discretization schemes for integral equations of hyperbolic problems are technically feasible and can yield promising results. However, the stability of the underlying collocation schemes is open. Numerical tests indicate that the proposed space-time collocation methods encounter similar stability issues as classical schemes. Further research in that direction is necessary to reveal correct formulations.

The major drawback of the presented approach is its increased demand in terms of computational resources compared to classical methods. This issue might spark further research on space-time discretization schemes. On the one hand, the proposed quadrature technique as well as its implementation could be improved. On the other hand, the development of fast methods, well-established in boundary element methods for elliptic problems, is a topic of research that seems to present itself.

Ultimately, one might consider the collocation method discussed in this work as a mere precursor to more involved Galerkin discretizations. However, their favourable properties in terms of stability come at the price of more intricate integrals in the computation of the Galerkin matrix entries. Nevertheless, our work presents a strong indication that space-time discretizations of boundary integral equations of hyperbolic problems have great potential.

A Proofs of the lemmas

Proof of Lemma 3.1. By the chain rule $\nabla(\phi \circ \chi_\tau(\xi)) = J_\tau^\top(\xi)\nabla\phi \circ \chi_\tau(\xi)$ holds when ϕ is differentiable at $\chi_\tau(\xi)$. Since ϕ is Lipschitz continuous it is differentiable almost everywhere by Rademacher's theorem. In particular, for $(\zeta, y) = \chi_\tau(\xi)$ it holds

$$\nabla\phi(\zeta, y) = \begin{bmatrix} 1 \\ -\frac{x-y}{\|x-y\|} \end{bmatrix} \quad , \quad \|\nabla\phi(\zeta, y)\|^2 = 2$$

when $x \neq y$. For simplicity of notation we omit the argument lists and the subscript τ. We set $q \coloneqq \nabla\phi$, hence

$$\|\nabla(\phi \circ \chi)\|^2 = \|J^\top q\|^2 = \left\langle J^\top q, J^\top q \right\rangle = \left\langle JJ^\top q, q \right\rangle.$$

To prove the lower bound, consider $z \coloneqq q - \langle q, \nu \rangle \nu$ where ν spans the kernel of $J^\top$. Since $\|\nu\| = 1$ it holds $\|z\|^2 = \|q\|^2 - \langle q, \nu \rangle^2 = 2 - \langle q, \nu \rangle^2$. From $\nu^\top = \begin{pmatrix} 0 & n^\top \end{pmatrix}$ and the Cauchy-Schwarz inequality it follows

$$|\langle q, \nu \rangle| = \left| \left\langle \frac{x-y}{\|x-y\|}, n \right\rangle \right| \leq 1$$

and we conclude

$$\|z\|^2 = 2 - \langle q, \nu \rangle^2 \geq 1. \tag{27}$$

Notice that the matrix $JJ^\top$ is (symmetric) positive semidefinite, consequently its normalized eigenvectors form an orthonormal basis. From $\operatorname{span}\{\nu\} = \ker J^\top$ it follows $\beta_1 = 0$ and $0 < \beta_2 \leq \beta_3 \leq \beta_4$ where $\beta_i, i = 1, \ldots, 4$ are the eigenvalues of $JJ^\top$. This enables the decomposition $JJ^\top = VCV^\top$ with $C \coloneqq \operatorname{diag}(\beta_i)_{i=1}^4$ and $V^\top = V^{-1}$ contains the normalized eigenvectors $\{\nu, e_2, e_3, e_4\}$. We obtain

$$\|\nabla(\phi \circ \chi)\|^2 = \left\langle JJ^\top q, q \right\rangle = \left\langle CV^\top q, V^\top q \right\rangle.$$

Since $q - z = \langle q, \nu \rangle \nu \in \ker J^\top$ it follows $CV^\top(q - z) = 0$ and

$$\left\langle CV^\top q, V^\top q \right\rangle = \left\langle CV^\top z, V^\top q \right\rangle = \left\langle V^\top z, CV^\top q \right\rangle = \left\langle CV^\top z, V^\top z \right\rangle.$$

Using the basis spanned by the normalized eigenvectors, the bound

$$\left\langle CV^\top z, V^\top z \right\rangle = \sum_{i=2}^4 \beta_i \langle z, e_i \rangle^2 \geq \beta_2 \sum_{i=2}^4 \langle z, e_i \rangle^2 = \beta_2 \|z\|^2 \tag{28}$$

follows, where the last equality is due to the expansion $\|z\|^2 = \sum_{i=2}^4 \langle z, e_i \rangle^2 + \langle z, \nu \rangle^2$ and $\langle z, \nu \rangle = 0$. Combination of Eq. (28) with Eq. (27) yields the asserted lower bound

$$\|\nabla(\phi \circ \chi)\|^2 = \left\langle CV^\top z, V^\top z \right\rangle \geq \beta_2 \|z\|^2 \geq \beta_2$$

The upper bound is due to the operator norm $\|J^\top q\|^2 \leq \beta_{\max}(JJ^\top)\|q\|^2 = 2\beta_4$. □

Proof of Lemma 3.2. The matrix A has the form $A = J^\top J - 2 j_t j_t^\top$, where $j_t \in \mathbb{R}^3$ is the first column of $J^\top$. From $\operatorname{rank} J = 3$ it follows that $J^\top J$ is positive definite, hence A can have at most one non-positive eigenvalue [30, p. 325], implying $0 < \lambda_2 \leq \lambda_3$. As a consequence A has exactly one negative eigenvalue iff there exists an $x \in \mathbb{R}^3$ such that $0 > \langle Ax, x\rangle = \langle MJx, Jx\rangle$. Equivalently, there has to exist an $y \in \operatorname{ran} J$ such that $\langle My, y\rangle < 0$. The vector $y \in \mathbb{R}^4$ is in $\operatorname{ran} J$ iff $0 = \langle y, \nu\rangle = y_t \nu_t + \langle y_x, \nu_x\rangle$, since the kernel of $J^\top$ is spanned by ν. Using $\nu_t = 0$ it follows

$$\lambda_1 < 0 \;\Leftrightarrow\; \exists y \in \mathbb{R}^4 : \langle y_x, \nu_x\rangle = 0 \;\wedge\; \langle My, y\rangle = \|y_x\|^2 - y_t^2 < 0.$$

Choosing $y = (\alpha, 0, 0, 0)^\top$, i.e. $y_t = \alpha \in \mathbb{R} \setminus \{0\}$ and $y_x = 0$ satisfies above condition. It follows $\lambda_1 < 0$, which proves the first part of the lemma. For the second part, note that A is invertible since no eigenvalue is zero. Consequently ξ_O is the unique solution of $A\xi_O = -b$ or by using $A = J^\top MJ$ and $b = -J^\top M z_0$

$$J^\top MJ\xi_O = J^\top M z_0 \;\Leftrightarrow\; J^\top M(J\xi_O - z_0) = 0.$$

It follows $M(J\xi_O - z_0) \in \ker J^\top$ or equivalently

$$\exists \beta \in \mathbb{R} : J\xi_O - z_0 = \beta M\nu \;\Leftrightarrow\; J\xi_O = z_0 + \beta M\nu \tag{29}$$

where we used $M = M^{-1}$. A solution to Eq. (29) exists iff the right hand side $z_0 + \beta M\nu$ is orthogonal to $\ker J^\top$. Since the solution of Eq. (29) is equivalent to the unique solution of $A\xi_O = -b$ the condition $\langle z_0 + \beta M\nu, \nu\rangle = 0$ must hold and from $\langle M\nu, \nu\rangle = 1$ follows $\beta = -\langle z_0, \nu\rangle$. Insertion into $c_M = c_0 + \langle b, \xi_O\rangle$ with $c_0 = \langle Mz_0, z_0\rangle$ yields

$$c_M = \langle Mz_0, z_0\rangle - \left\langle J^\top M z_0, \xi_O \right\rangle = \langle Mz_0, z_0 - J\xi_O\rangle = -\beta \langle Mz_0, M\nu\rangle = \langle z_0, \nu\rangle^2$$

which proves the assertion. □

Proof of Lemma 3.3. For any $\rho \in \operatorname{dom} \psi$ the transformation determinant reads

$$g_\psi(\rho) = \left(\|\partial_1 \psi(\rho)\|^2 \|\partial_2 \psi(\rho)\|^2 - \langle \partial_1 \psi(\rho), \partial_2 \psi(\rho)\rangle^2 \right)^{1/2}.$$

Set $X = C$ when $c_M = 0$ or $X = H$ when $c_M > 0$. The chain rule in conjunction with the orthogonality of the eigenvectors of A, i.e. $E^\top = E^{-1}$ yields

$$\left\langle \partial_i \psi(\rho), \partial_j \psi(\rho) \right\rangle = \left\langle E\partial_i \psi_X(\rho), E\partial_j \psi_X(\rho) \right\rangle = \left\langle \partial_i \psi_X(\rho), \partial_j \psi_X(\rho) \right\rangle, \quad i, j = 1, 2.$$

For $c_M = 0$ the asserted representation of g_ψ follows by computing the partial derivatives of ψ_C with

$$g_C(\rho) = \left[\left(\tfrac{\sin^2 \rho_1}{\lambda_2} + \tfrac{\cos^2 \rho_1}{\lambda_3} \right) \left(\tfrac{1}{-\lambda_1} + \tfrac{\cos^2 \rho_1}{\lambda_2} + \tfrac{\sin^2 \rho_1}{\lambda_3} \right) - \tfrac{(\lambda_3 - \lambda_2)^2}{\lambda_2^2 \lambda_3^2} \sin^2 \rho_1 \cos^2 \rho_1 \right]^{1/2}.$$

For $c_M > 0$ the asserted formula for g_ψ is obtained via the partial derivatives of ψ_H with

$$g_H(\rho) = \left[\left(\tfrac{\sin^2 \rho_1}{\lambda_2} + \tfrac{\cos^2 \rho_1}{\lambda_3} \right) \left(\tfrac{\tanh^2 \rho_2}{-\lambda_1} + \tfrac{\cos^2 \rho_1}{\lambda_2} + \tfrac{\sin^2 \rho_1}{\lambda_3} \right) - \tfrac{(\lambda_3 - \lambda_2)^2}{\lambda_2^2 \lambda_3^2} \sin^2 \rho_1 \cos^2 \rho_1 \right]^{1/2}$$

from which the first part of the theorem follows. As we direct our attention towards the second part, consider an arbitrary but fixed $\rho \in \operatorname{dom}\psi$ and set

$$\eta := \psi_X(\rho) \quad , \quad \xi := \kappa(\eta) = \kappa \circ \psi_X(\rho) \quad , \quad \begin{pmatrix} \zeta \\ y \end{pmatrix} := \begin{pmatrix} |_t\chi(\xi) \\ |_x\chi(\xi) \end{pmatrix} = \chi(\xi) = \chi \circ \kappa \circ \psi_X(\rho).$$

Since $(\zeta, y) \in \Xi$ it follows

$$d_x(y) = \|x-y\| = t - \zeta = t - t_0 - j_t^\top \xi = t - t_0 - j_t^\top \xi_O - j_t^\top E\eta$$

where we used the explicit representations of the affine maps χ and κ. By Eq. (29) there exists a $\beta \in \mathbb{R}$ such that $t - t_0 - j_t^\top \xi_O = \beta v_t$. Since $v_t = 0$ it follows

$$d_x(y) = -j_t^\top E\eta = -\sum_{i=1}^{3} \langle j_t, e_i \rangle \, \eta_i.$$

Insertion of $\eta = \psi_C(\rho)$ for $c_M = 0$ and $\eta = \psi_H(\rho)$ for $c_M > 0$ yields the asserted representations of the distance function with

$$\begin{aligned} f_C(\rho) &= -\tfrac{\langle e_1, j_t \rangle}{\sqrt{-\lambda_1}} - \tfrac{\langle e_2, j_t \rangle}{\sqrt{\lambda_2}} \cos\rho_1 - \tfrac{\langle e_3, j_t \rangle}{\sqrt{\lambda_3}} \sin\rho_1, \\ f_H(\rho) &= -\tfrac{\langle e_1, j_t \rangle}{\sqrt{-\lambda_1}} - \tanh\rho_2 \left(\tfrac{\langle e_2, j_t \rangle}{\sqrt{\lambda_2}} \cos\rho_1 + \tfrac{\langle e_3, j_t \rangle}{\sqrt{\lambda_3}} \sin\rho_1 \right). \end{aligned}$$

By

$$\min_{\rho_1 \in \mathbb{R}} \left(-\tfrac{\langle e_2, j_t \rangle}{\sqrt{\lambda_2}} \cos\rho_1 - \tfrac{\langle e_3, j_t \rangle}{\sqrt{\lambda_3}} \sin\rho_1 \right) = -\left(\tfrac{\langle e_2, j_t \rangle^2}{\lambda_2} + \tfrac{\langle e_3, j_t \rangle^2}{\lambda_3} \right)^{1/2}$$

we obtain

$$f_X(\rho) \geq -\tfrac{\langle e_1, j_t \rangle}{\sqrt{-\lambda_1}} - \left(\tfrac{\langle e_2, j_t \rangle^2}{\lambda_2} + \tfrac{\langle e_3, j_t \rangle^2}{\lambda_3} \right)^{1/2}. \tag{30}$$

With the diagonalization $A = EDE^\top$ introduced in Section 3.2 it holds $A^{-1} = ED^{-1}E^\top$. Let $v \in \mathbb{R}^3$ be the unique solution of $Av = j_t$ and it follows

$$\langle v, j_t \rangle = \left\langle A^{-1} j_t, j_t \right\rangle = \left\langle D^{-1}E^\top j_t, E^\top j_t \right\rangle = \sum_{i=1}^{3} \frac{\langle e_i, j_t \rangle^2}{\lambda_i}. \tag{31}$$

Using the representation $A = J_x^\top J_x - j_t j_t^\top$ and $\dim\ker J_x = 1$ we obtain

$$v \in \ker J_x : \langle v, j_t \rangle = -1 \quad \Rightarrow \quad Av = J_x^\top J_x v - \langle v, j_t \rangle \, j_t = j_t. \tag{32}$$

Note that the solution in Eq. (32) exists, since j_t cannot be orthogonal to $0 \neq v \in \ker J_x$ as this would imply $Av = 0$ which violates Lemma 3.2 (A does not have a zero eigenvalue). Consequently, Eq. (32) is the unique solution of $Av = j_t$ and with Eq. (31)

$$\sum_{i=1}^{3} \frac{\langle e_i, j_t \rangle^2}{\lambda_i} = -1 \quad \Leftrightarrow \quad \frac{\langle e_i, j_t \rangle^2}{-\lambda_i} = 1 + \sum_{i=2}^{3} \frac{\langle e_i, j_t \rangle^2}{\lambda_i}$$

follows. The estimate Eq. (30) in conjunction with $\langle e_1, j_t \rangle < 0$ yields

$$f_X(\rho) \geq \left(1 + \tfrac{\langle e_2, j_t \rangle^2}{\lambda_2} + \tfrac{\langle e_3, j_t \rangle^2}{\lambda_3} \right)^{1/2} - \left(\tfrac{\langle e_2, j_t \rangle^2}{\lambda_2} + \tfrac{\langle e_3, j_t \rangle^2}{\lambda_3} \right)^{1/2}$$

which completes the proof. □

B Construction of Λ_1

A crucial component of the integration scheme proposed in Section 3.4 is a first-order approximation Λ_1 sufficiently close to $\Lambda = \psi^{-1}(\partial\hat{\tau} \cap \operatorname{ran}\psi)$. Let $\mathscr{F} = \{f_i\}_{i=1}^4$ be the set of four triangular faces of the reference tetrahedron $\hat{\tau}$, which leads to

$$\partial\hat{\tau} \cap \operatorname{ran}\psi = \bigcup_{f\in\mathscr{F}} f \cap \operatorname{ran}\psi.$$

Moreover, let $P_f \supset f$ be the plane induced by the three vertices of the triangle $f \in \mathscr{F}$. As discussed in Section 3.3 $\operatorname{ran}\psi$ is either a cone or one sheet of a two-sheeted hyperboloid. Consequently, $P_f \cap \operatorname{ran}\psi$ is a planar section through a cone/hyperboloid. This intersection is known, i.e. it is either a hyperbola, a parabola, an ellipse, or degenerate versions of them (unless it is empty). In any case, a (bijective) parametrization $\omega_f : \operatorname{dom}\omega \to P_f \cap \operatorname{ran}\psi$ with $\operatorname{dom}\omega_f \subseteq \mathbb{R}$ is available. The relevant subset of the parameter line $I_f = \omega_f^{-1}(f \cap \operatorname{ran}\psi)$ is obtained via following procedure. Let $\{r_i\}_{i=1}^{n_f} = \omega_f^{-1}(\partial f \cap \operatorname{ran}\psi)$ be the set of parameter points where the boundary of the triangle f (composed of three lines) intersects the quadric $\operatorname{ran}\psi$. Assume that these values are sorted in ascending order, i.e. $r_i < r_{i+1}$, then

$$I_f = \bigcup_{\substack{i=1,\dots,n_f:\\ \omega_f\left(\frac{1}{2}(r_i+r_{i+1})\right)\in f}} (r_i, r_{i+1}). \tag{33}$$

Note that, since ∂f is composed of line segments, computing $\partial f \cap \operatorname{ran}\psi$ amounts to solving quadratic equations in one variable. This can be implemented efficiently by a numerically stable version of the quadratic formula.

Next, the parametrization ω_f is evaluated at a few points to generate points from which the line elements of Λ_1 are built. To this end, consider the set of start points $\{s_i^A\}_{i=1}^{m_f}$ and end points $\{s_i^B\}_{i=1}^{m_f}$ such that

$$\overline{I_f} = \bigcup_{i=1}^{m_f} [s_i^A, s_i^B]$$

with the number of segments $m_f \in \mathbb{N}$. These points are obtained by uniform partitioning of the intervals in Eq. (33). A set of of line elements $\Lambda_1^f = \{\sigma_i\}_{i=1}^{m_f}$ is obtained by computing

$$\operatorname{dom}\psi \ni \rho_{\sigma_i}^* = \psi^{-1} \circ \omega_f(s_i^*), \quad i = 1,\dots,m_f, * \in \{A,B\}$$

and using $\rho_{\sigma_i}^A$ as start point and $\rho_{\sigma_i}^B$ as end point. As already indicated, each line element has to be sufficiently close to Λ. To quantify proximity, we use the condition

$$|\sigma_i| \leq c_K \inf_{s\in(s_i^A, s_i^B)} \frac{1}{\kappa_\Lambda(\psi^{-1} \circ \omega_f(s))} \tag{34}$$

where $\kappa_\Lambda(\rho)$ is the curvature of Λ at $\rho \in \Lambda$ and $c_K > 0$. Condition Eq. (34) implies that the length of the line element σ_i is not greater than the minimal radius of curvature along the corresponding subset of Λ scaled by the positive constant c_K. If an element σ_i does not satisfy Eq. (34) it is

refined by adding the point $\frac{1}{2}(s_i^A + s_i^B)$ to the list of start and end points, until the criterion is met. Note that in our implementation the infimum in Eq. (34) is not computed exactly, but the minimum of a fixed number, say 10, of equally spaced sampling points is used. To compensate this (at least to some extent) we use $c_K < 1$, in particular $c_K = 1/2$, in all of the conducted tests. Finally, the set of line elements Λ_1 is obtained by collecting the line elements obtained through this procedure for every face, i.e. $\Lambda_1 = \bigcup_{f \in \mathscr{F}} \Lambda_1^f$.

Acknowledgments

We greatly appreciate the discussions with M.H. Gfrerer, G. Of, and M. Zank. Our exchanges shaped several ideas uttered in this publication.

References

[1] A. Aimi, M. Diligenti, A. Frangi, and C. Guardasoni. A stable 3d energetic galerkin bem approach for wave propagation interior problems. *Eng. Anal. Bound. Elem.*, 36(12):1756–1765, 2012. doi: 10.1016/j.enganabound.2012.06.003.

[2] A. Aimi, M. Diligenti, A. Frangi, and C. Guardasoni. Neumann exterior wave propagation problems: computational aspects of 3d energetic galerkin bem. *Comput. Mech.*, 51(4): 475–493, 2013. doi: 10.1007/s00466-012-0796-5.

[3] J. Ballani, L. Banjai, S. Sauter, and A. Veit. Numerical solution of exterior maxwell problems by galerkin bem and runge-kutta convolution quadrature. *Numer. Math.*, 123(4): 643–670, 2013. doi: 10.1007/s00211-012-0503-7.

[4] A. Bamberger and T. Ha Duong. Formulation variationnelle espace-temps pour le calcul par potentiel retardé de la diffraction d'une onde acoustique (i). *Math. Methods Appl. Sci.*, 8(1):405–435, 1986. doi: doi:10.1002/mma.1670080127.

[5] A. Bamberger and T. Ha Duong. Formulation variationnelle pour le calcul de la diffraction d'une onde acoustique par une surface rigide. *Math. Methods Appl. Sci.*, 8(4):598–608, 1986. doi: 10.1002/mma.1670080139.

[6] L. Banjai and S. Sauter. Rapid solution of the wave equation in unbounded domains. *SIAM J. Numer. Anal.*, 47(1):227–249, 2009. doi: 10.1137/070690754.

[7] L. Banjai and M. Schanz. Wave propagation problems treated with convolution quadrature and bem. In U. Langer, M. Schanz, O. Steinbach, and W.L. Wendland, editors, *Fast Boundary Element Methods in Engineering and Industrial Applications*, pages 145–184. Springer Berlin Heidelberg, Berlin, Heidelberg, 2012. ISBN 978-3-642-25670-7. doi: 10.1007/978-3-642-25670-7_5.

[8] L. Banz, H. Gimperlein, Z. Nezhi, and E.P. Stephan. Time domain bem for sound radiation of tires. *Comput. Mech.*, 58(1):45–57, 2016. doi: 10.1007/s00466-016-1281-3.

[9] M. Behr. Simplex space-time meshes in finite element simulations. *Internat. J. Numer. Methods Fluids*, 57(9):1421–1434, 2008. doi: 10.1002/fld.1796.

[10] M.J. Bluck and S.P. Walker. Analysis of three-dimensional transient acoustic wave propagation using the boundary integral equation method. *Internat. J. Numer. Methods Engrg.*, 39(8):1419–1431, 1996. doi: 10.1002/(SICI)1097-0207(19960430)39:8<1419::AID-NME911>3.0.CO;2-C.

[11] M. Costabel and F.-J. Sayas. Time-dependent problems with the boundary integral equation method. *Encycl. Comput. Mech. Second Ed.*, 2:1–24, 2017. doi: 10.1002/9781119176817.ecm2022.

[12] P. Davies and D. Duncan. Stability and convergence of collocation schemes for retarded potential integral equations. *SIAM J. Numer. Anal.*, 42(3):1167–1188, 2004. doi: 10.1137/S0036142901395321.

[13] P.J. Davies. A stability analysis of a time marching scheme for the general surface electric field integral equation. *Appl. Numer. Math.*, 27(1):33–57, 1998. doi: 10.1016/S0168-9274(97)00107-4.

[14] P.J. Davies and D.B. Duncan. Averaging techniques for time-marching schemes for retarded potential integral equations. *Appl. Numer. Math.*, 23(3):291–310, 1997. doi: 10.1016/S0168-9274(96)00069-4.

[15] L. Demkowicz, J. Gopalakrishnan, S. Nagaraj, and P. Sepúlveda. A spacetime dpg method for the schrödinger equation. *SIAM J. Numer. Anal.*, 55(4):1740–1759, 2017. doi: 10.1137/16M1099765.

[16] A. Demlow and G. Dziuk. An adaptive finite element method for the laplace-beltrami operator on implicitly defined surfaces. *SIAM J. Numer. Anal.*, 45(1):421–442, 2007. doi: 10.1137/050642873.

[17] S. Dohr, K. Niino, and O. Steinbach. Space-time boundary element methods for the heat equation, 2018.

[18] W. Dörfler, S. Findeisen, and C. Wieners. Space-time discontinuous galerkin discretizations for linear first-order hyperbolic evolution systems. *Comput. Methods Appl. Math.*, 16 (3):409–428, 2016. doi: 10.1515/cmam-2016-0015.

[19] H. Federer. Curvature measures. *Trans. Amer. Math. Soc.*, 93(3):418–491, 1959. doi: 10.1090/S0002-9947-1959-0110078-1.

[20] P. Foteinos and N. Chrisochoides. 4d space-time delaunay meshing for medical images. *Eng. Comput.*, 31(3):499–511, 2015. ISSN 1435-5663. doi: 10.1007/s00366-014-0380-z.

[21] M.B. Friedman and R. Shaw. Diffraction of pulses by cylindrical obstacles of arbitrary cross section. *J. Appl. Mech.*, 29(1):40–46, 1962. doi: 10.1115/1.3636495.

[22] T.-P. Fries and S. Omerović. Higher-order accurate integration of implicit geometries. *Internat. J. Numer. Methods Engrg.*, 106(5):323–371, 2016. doi: 10.1002/nme.5121.

[23] T.P. Fries, Omerović, D. Schöllhammer, and J. Steidl. Higher-order meshing of implicit geometries-part i: Integration and interpolation in cut elements. *Comput. Methods Appl. Mech. Engrg.*, 313:759–784, 2017. doi: 10.1016/j.cma.2016.10.019.

[24] M. Gander and M. Neumüller. Analysis of a new space-time parallel multigrid algorithm for parabolic problems. *SIAM J. Sci. Comput.*, 38(4):A2173–A2208, 2016. doi: 10.1137/15M1046605.

[25] M.H. Gfrerer and M. Schanz. A high-order fem with exact geometry description for the laplacian on implicitly defined surfaces. *Internat. J. Numer. Methods Engrg.*, 114(11):1163–1178, 2018. doi: 10.1002/nme.5779.

[26] H. Gimperlein and D. Stark. Algorithmic aspects of enriched time domain boundary element methods. *Eng. Anal. Bound. Elem.*, 2018. doi: 10.1016/j.enganabound.2018.02.010. Article in Press.

[27] H. Gimperlein, M. Maischak, and E.P. Stephan. Adaptive time domain boundary element methods with engineering applications. *J. Integral Equations Appl.*, 29(1):75–105, 2017. doi: 10.1216/JIE-2017-29-1-75.

[28] H. Gimperlein, F. Meyer, C. Özdemir, D. Stark, and E.P. Stephan. Boundary elements with mesh refinements for the wave equation. *Numer. Math.*, 139(4):867–912, 2018. doi: 10.1007/s00211-018-0954-6.

[29] M. Gläfke. *Adaptive Methods for Time Domain Boundary Integral Equations*. PhD thesis, Brunel University London, 2012.

[30] G. Golub. Some modified matrix eigenvalue problems. *SIAM Rev.*, 15(2):318–334, 1973. doi: 10.1137/1015032.

[31] J. Gopalakrishnan and P. Sepúlveda. A spacetime dpg method for the wave equation in multiple dimensions, 2017.

[32] J. Gopalakrishnan, J. Schöberl, and C. Wintersteiger. Mapped tent pitching schemes for hyperbolic systems. *SIAM J. Sci. Comput.*, 39(6):B1043–B1063, 2017. doi: 10.1137/16M1101374.

[33] T. Ha-Duong. On retarded potential boundary integral equations and their discretisation. In M. Ainsworth, P. Davies, D. Duncan, B. Rynne, and P. Martin, editors, *Topics in Computational Wave Propagation*, volume 31, pages 301–336. Springer Berlin Heidelberg, Berlin, Heidelberg, 2003. doi: 10.1007/978-3-642-55483-4_8.

[34] G.M. Hulbert and T.J.R. Hughes. Space-time finite element methods for second-order hyperbolic equations. *Comput. Methods Appl. Mech. Engrg.*, 84(3):327–348, 1990. doi: 10.1016/0045-7825(90)90082-W.

[35] P. Joly and J. Rodríguez. Mathematical aspects of variational boundary integral equations for time dependent wave propagation. *J. Integral Equations Appl.*, 29(1):137–187, 2017. doi: 10.1216/JIE-2017-29-1-137.

[36] E. Karabelas and M. Neumüller. Generating admissible space-time meshes for moving domains in $d+1$-dimensions, 2015.

[37] L. Kudela, N. Zander, T. Bog, S. Kollmannsberger, and E. Rank. Efficient and accurate numerical quadrature for immersed boundary methods. *Adv. Model. and Simul. in Eng. Sci.*, 2(1):10, 2015. ISSN 2213-7467. doi: 10.1186/s40323-015-0031-y.

[38] C. Lehrenfeld. High order unfitted finite element methods on level set domains using isoparametric mappings. *Comput. Methods Appl. Mech. Engrg.*, 300:716–733, 2016. doi: 10.1016/j.cma.2015.12.005.

[39] M. Lopez-Fernandez and S. Sauter. Generalized convolution quadrature with variable time stepping. *IMA J. Numer. Anal.*, 33(4):1156–1175, 2013. doi: 10.1093/imanum/drs034.

[40] M. Lopez-Fernandez and S. Sauter. Generalized convolution quadrature with variable time stepping. part ii: Algorithm and numerical results. *Appl. Numer. Math.*, 94:88–105, 2015. doi: 10.1016/j.apnum.2015.03.004.

[41] M. Lopez-Fernandez and S. Sauter. Generalized convolution quadrature based on runge-kutta methods. *Numer. Math.*, 133(4):743–779, 2016. doi: 10.1007/s00211-015-0761-2.

[42] C. Lubich. Convolution quadrature and discretized operational calculus. i. *Numer. Math.*, 52(2):129–145, 1988. doi: 10.1007/BF01398686.

[43] C. Lubich. Convolution quadrature and discretized operational calculus. ii. *Numer. Math.*, 52(4):413–425, 1988. doi: 10.1007/BF01462237.

[44] C. Lubich. On the multistep time discretization of linear initial-boundary value problems and their boundary integral equations. *Numer. Math.*, 67(3):365–389, 1994. doi: 10.1007/s002110050033.

[45] N. Manson and J. Tausch. Quadrature for parabolic galerkin bem with moving surfaces. *Comput. Math. Appl.*, 77(1):1–14, 2019. doi: 10.1016/j.camwa.2018.09.004.

[46] Webe João Mansur. *A time-stepping technique to solve wave propagation problems using the boundary element method*. PhD thesis, University of Southampton, 1983.

[47] W.J. Mansur and C.A. Brebbia. Numerical implementation of the boundary element method for two dimensional transient scalar wave propagation problems. *Appl. Math. Model.*, 6(4):299–306, 1982. doi: 10.1016/S0307-904X(82)80038-3.

[48] B. Müller, F. Kummer, and M. Oberlack. Highly accurate surface and volume integration on implicit domains by means of moment-fitting. *Internat. J. Numer. Methods Engrg.*, 96 (8):512–528, 2013. doi: 10.1002/nme.4569.

[49] M. Neumüller. *Space-Time Methods: Fast Solvers and Applications*. PhD thesis, Graz University of Technology, 2013.

[50] M. Neumüller, P.S. Vassilevski, and U.E. Villa. Space-time cfosls methods with amge upscaling. In C.-O. Lee, X.-C. Cai, D.E. Keyes, H.H. Kim, A. Klawonn, E.-J. Park, and O.B. Widlund, editors, *Domain Decomposition Methods in Science and Engineering XXIII*, volume 116, pages 253–260, Cham, 2017. Springer International Publishing. doi: 10.1007/978-3-319-52389-7_25.

[51] N. Ortner. Regularisierte faltung von distributionen. teil 2: Eine tabelle von fundamentallösungen. *Z. Angew. Math. Phys.*, 31(1):155–173, 1980. doi: 10.1007/BF01601710.

[52] N. Ortner and P. Wagner. *Fundamental Solutions of Linear Partial Differential Operators: Theory and Practice*. Springer, Cham, 2015. doi: 10.1007/978-3-319-20140-5.

[53] D. Pölz, M.H. Gfrerer, and M. Schanz. Wave propagation in elastic trusses: An approach via retarded potentials. *Wave Motion*, 2018. doi: 10.1016/j.wavemoti.2018.06.002. Article in Press.

[54] W.H. Press, S.A. Teukolsky, W.T. Vetterling, and B.P. Flannery. *Numerical Recipes: The Art of Scientific Computing*. Cambridge University Press, Cambridge, UK, 3 edition, 2007.

[55] E. Rothe. Zweidimensionale parabolische randwertaufgaben als grenzfall eindimensionaler randwertaufgaben. *Math. Ann.*, 102(1):650–670, 1930. doi: 10.1007/BF01782368.

[56] B.P. Rynne. Instabilities in time marching methods for scattering problems. *Electromagnetics*, 6(2):129–144, 1986. doi: 10.1080/02726348608915207.

[57] B.P. Rynne. Time domain scattering from arbitrary surfaces using the electric field integral equation. *J. Electromagn. Waves Appl.*, 5(1):93–112, 1991. doi: 10.1163/156939391X00491.

[58] B.P. Rynne. The well-posedness of the electric field integral equation for transient scattering from a perfectly conducting body. *Math. Methods Appl. Sci.*, 22(7):619–631, 1999. doi: 10.1002/(SICI)1099-1476(19990510)22:7<619::AID-MMA59>3.0.CO;2-E.

[59] B.P. Rynne and P.D. Smith. Stability of time marching algorithms for the electric field integral equation. *J. Electromagn. Waves Appl.*, 4(12):1181–1205, 1990. doi: 10.1163/156939390X00762.

[60] S. Sauter and A. Veit. A galerkin method for retarded boundary integral equations with smooth and compactly supported temporal basis functions. *Numer. Math.*, 123(1):145–176, 2013. doi: 10.1007/s00211-012-0483-7.

[61] S. Sauter and A. Veit. Adaptive time discretization for retarded potentials. *Numer. Math.*, 132(3):569–595, 2016. doi: 10.1007/s00211-015-0726-5.

[62] S.A. Sauter and C. Schwab. *Boundary Element Methods*, volume 39 of *Springer Series in Computational Mathematics*. Springer Berlin Heidelberg, 2011. doi: 10.1007/978-3-540-68093-2.

[63] F.-J. Sayas. Energy estimates for galerkin semidiscretizations of time domain boundary integral equations. *Numer. Math.*, 124(1):121–149, 2013. doi: 10.1007/s00211-012-0506-4.

[64] F.-J. Sayas. *Retarded Potentials and Time Domain Boundary Integral Equations: A Road Map*, volume 50 of *Springer Series in Computational Mathematics*. Springer, Cham, 2016. doi: 10.1007/978-3-319-26645-9.

[65] R. Saye. High-order quadrature methods for implicitly defined surfaces and volumes in hyperrectangles. *SIAM J. Sci. Comput.*, 37(2):A993–A1019, 2015. doi: 10.1137/140966290.

[66] M. Schanz. *Wave Propagation in Viscoelastic and Poroelastic Continua: A Boundary Element Approach*, volume 2 of *Lecture Notes in Applied and Computational Mechanics*. Springer-Verlag Berlin Heidelberg, 2001. doi: 10.1007/978-3-540-44575-3.

[67] O. Steinbach. Space-time finite element methods for parabolic problems. *Comput. Methods Appl. Math.*, 15(4):551–566, 2015. doi: 10.1515/cmam-2015-0026.

[68] A. Veit, M. Merta, J. Zapletal, and D. Lukáš. Efficient solution of time-domain boundary integral equations arising in sound-hard scattering. *Internat. J. Numer. Methods Engrg.*, 107(5):430–449, 2016. doi: 10.1002/nme.5187.

[69] K. Voronin, C.S. Lee, M. Neumüller, P. Sepulveda, and P.S. Vassilevski. Space-time discretizations using constrained first-order system least squares (cfosls). *J. Comput. Phys.*, 373:863–876, 2018. doi: 10.1016/j.jcp.2018.07.024.

[70] L. Wang and P.-O. Persson. A high-order discontinuous galerkin method with unstructured spaceâĂŞtime meshes for two-dimensional compressible flows on domains with large deformations. *Comput. & Fluids*, 118:53–68, 2015. ISSN 0045-7930. doi: 10.1016/j.compfluid.2015.05.026.

[71] M. Zank and O. Steinbach. Adaptive space-time boundary element methods for the wave equation. *PAMM. Proc. Appl. Math. Mech.*, 16(1):777–778, 2016. doi: 10.1002/pamm.201610377.